THE UNIVERSITY OF CHICAGO

NOckout: A DNA-BASED FLUORESCENT PROBE TO QUANTITATIVELY MAP NOS3 ACTIVITY WITH SUBCELLULAR SPATIAL RESOLUTION

A DISSERTATION SUBMITTED TO

THE FACULTY OF THE DIVISION OF THE PHYSICAL SCIENCES

IN CANDIDACY FOR THE DEGREE OF

DOCTOR OF PHILOSOPHY

DEPARTMENT OF CHEMISTRY

BY

MAULIK SUBHASH JANI

CHICAGO, ILLINOIS

AUGUST 2020

Table of Contents

List of Figures

List of tables

Acknowledgements

I am grateful to many people who helped me during this journey and made it an amazing experience, I wish to take this opportunity to acknowledge them. First and foremost, I would like to express very great appreciation and thank my doctoral advisor Prof. Yamuna Krishnan. I have always been inspired by her appealing confidence and ambitions, her hard work, devotion to the lab, continuous enthusiasm for challenging problems and her genuine care for students. Yamuna gave me complete intellectual freedom and trusted me from the start to test various challenging problems. I learnt a lot, both personally and professionally from Yamuna, especially science communication and writing, I would not be where I am without her constant support and mentoring.

I would like to thank my collaborator and thesis committee member Prof. Yun Fang for his critical and helpful insight into my work. Yun was always available to meet and discuss whenever I needed to, whether its guidance and tips during paper revision or to answer my never-ending questions about academia. Despite of his busy schedule he has always helped me troubleshoot biochemical assays without which this work could not have been completed. I would also like to thank my thesis committee member Prof. Raymond Moellering for insightful and though-provoking discussions on the project and on science in general. I have always been inspired by the problems that he works on and the unique way that he looks at chemical biology.

I would like to thank Aneesh for all the life advices, mentoring, being an amazing collaborator and a true friend both inside and outside of the lab. He has taught me great deal of soft skills as well as hard skills, NOS projects would have been impossible without him. I also thank Aneesh and Ambili for their hospitality and amazing food. I would like to thank Shareefa for insightful scientific and political discussions, selfless help with chores inside and outside of the lab and being

an amazing friend. I would like to thank Ved for his help with technical difficulties in the lab and transferring some of his technical skills. Ved and Shareefa both were amazing apartment mates and all the fun things that we did together made the transition smoother. I would also like to thank Junyi for the insightful discussions and troubleshooting skills which made the enzyme activity quantification possible. I would also like to mention those 2AM Diablo rift runs, concerts and china town trips, gym sessions with John etc. which made this journey fun and joyful. Shabana and Saikat helped me with experiments and understanding lab culture when I started at NCBS. Shabana has been a wonderful friend, I thank her for all the scientific and non-scientific discussions, amazing food and for being cubicle buddy both at NCBS and at UChicago. I would also like to thank Kasturi, Anand, Bhavya and KaHo for being amazing hosts, friends and game buddies, their scientific and non-scientific inputs, tips and discussions have made this journey lively and smoother. I would also like to thank all the past members of Krishna lab, Drs' Sunaina, Sonali, Suruchi, Dhiraj, Saheli, Masood, Nagarjun, Krishna for being supportive, discussing science at a very high level and helping me grow in many ways. I would like to thank Matt for being a good friend, correcting almost all of my scientific writings and for all the scientific and otherwise discussions that helped me a lot during this journey. I would like to thank Devin and Eunie for being amazing apartment mates, great friends, for making me familiar with US culture and sports and all the fun things that we did together which made this journey joyful. I would like to thank Rahul, Xiao, Hiling, Jin, Julia, Jane, Kaitlin, Simon, Siggy, Tong for being amazing neighbors, generous suppliers and tips and tricks to make experiments work. I would like to thank Rahul and Anwesha for being great friends, amazing hosts, for all the stimulating discussions and great food.

I would like to thank my family for being source of great comfort and care. I would like to also thank Sanjay and Hema (Masa-Masi) for their love, support, for always being there, for amazing hospitality and great food. I would like to acknowledge and show my utmost gratitude to Papa, Mummy and Jahanvi for unconditional love and support during every moment of my life, for giving me wings to fly, for always being source of my energy, inspiration and positivity. I would not have been anywhere without their constant support. Last but not the least, I would like to thank love of my life Shrunali, her unconditional love, constant support, continuous care, encouragement and understanding have made me a better person and immensely helped me during this journey. I am lucky to have her and cannot imagine life without her.

Abstract

Compartmentalized nitric oxide (NO) production drives critical signaling pathways in cells, yet there are no methods to quantitatively image NO with sub-cellular spatial resolution in living systems. Here, we introduce a new DNA-based fluorescent reporter technology that maps NO with sub-cellular resolution in live cells. It combines small molecule NO detection chemistry with the sub-cellular targetability of DNA based scaffold to provide quantifiable NO maps using ratiometric imaging. We could thereby map the activity of Nitric Oxide Synthase 3 (NOS3) which resides at the plasma membrane and the trans-Golgi network. We find that despite its lower abundance, the pool of NOS3 at the plasma membrane is seven-fold more active than Golgi associated NOS3. The ability to quantitatively map NO dynamics with sub-cellular resolution provides the potential to discover selective regulators of distinct NOS3 populations.

List of publications

1. Veetil, A.T., Zou, J.[#], Henderson, K.W. [#], **Jani, M.S.** [#], Shaik, S.M., Sisodia, S.S., Hale M.E. and Krishnan, Y. (2020) ***Proc. Natl. Acad. Sci. USA*** (In print). [#] equal contributions.

2. **Jani, M.S.**, Zou, J., Veetil, A.T., and Krishnan, Y. (2020). A DNA-based fluorescent probe maps NOS3 activity with subcellular spatial resolution. ***Nat. Chem. Biol.*** 16, 660–666.

3. **Jani, M.S.**, T. Veetil, A., and Krishnan, Y. (2020). Controlled release of bioactive signaling molecules. ***Methods in Enzymology*** 638, 2020, Pages 129-138.

4. **Jani, M.S.**, Veetil, A.T., and Krishnan, Y. (2019). Precision immunomodulation with synthetic nucleic acid technologies. ***Nat. Rev. Mater.*** 4, pages451–458

5. Thekkan, S., **Jani, M.S.**, Cui, C., Dan, K., Zhou, G., Becker, L., and Krishnan, Y. (2019). A DNA-based fluorescent reporter maps HOCl production in the maturing phagosome. ***Nat. Chem. Biol.*** 15, 1165–1172.

6. Veetil, A.T., **Jani, M.S.**, and Krishnan, Y. (2018). Chemical control over membrane-initiated steroid signaling with a DNA nanocapsule. ***Proc. Natl. Acad. Sci. USA*** 115, 9432–9437.

Chapter 1

Introduction

1.1 Nitric Oxide: A versatile signaling molecule:

Nitric oxide (NO) is a lipophilic, highly reactive and small endogenous second messenger that regulates a number of important signaling pathways. NO regulates blood pressure by controlling vascular tone, synaptic plasticity by acting as retrograde neurotransmitter and helps in host defense through its bactericidal and cytostatic activities[1–5]. NO is a short lived, highly diffusible and is a radical species and, due to these properties, it cannot be stored and released like most other second messenger molecules[6,7]. Therefore, NO production is regulated tightly in space and time, the dysregulation of which leads to diverse pathophysiological conditions[3,6,8].

NO is produced by a family of enzymes called Nitric Oxide Synthases (NOS). Humans have three NOS isoforms: neuronal NOS (nNOS or NOS1), inducible NOS (iNOS or NOS2) and endothelial NOS (eNOS or NOS3)[3,9]. All NOS isoforms function as homodimers, use L-arginine and O_2 as substrates and require a number of co-factors, such as flavin mononucleotide (FMN), nicotinamide-adenine-dinucleotide phosphate (reduced NADPH), flavin adenine dinucleotide (FAD), tetrahydrobiopterin (BH_4) and heme[10–12]. NOS isoforms transfer electrons from the C-terminal reductase domain through NADPH to FAD to FMN to the heme center of the N-terminal oxygenase domain of NOS3 (Fig. 1.1). Beside heme, the oxygenase domain also contains BH_4 and a binding site for the substrate L-arginine[11,13]. This electron transfer directed towards the heme center is used to reduce O_2 and oxidize L-arginine to yield L-citrulline via an N^{ω}-hydroxy-L-arginine intermediate and a molecule of NO (Fig. 1.1)[12,14].

All three NOS isoforms have a calmodulin binding site. In the case of NOS1 and NOS3, an increase in cytoplasmic calcium levels mediates calmodulin binding. This calmodulin binding event facilitates electron flow from the reductase domain to the oxygenase domain and increases NOS efficiency to produce NO. On the other hand, NOS2 can bind calmodulin even when intracellular calcium levels are as low as 40 nM.[10,15]

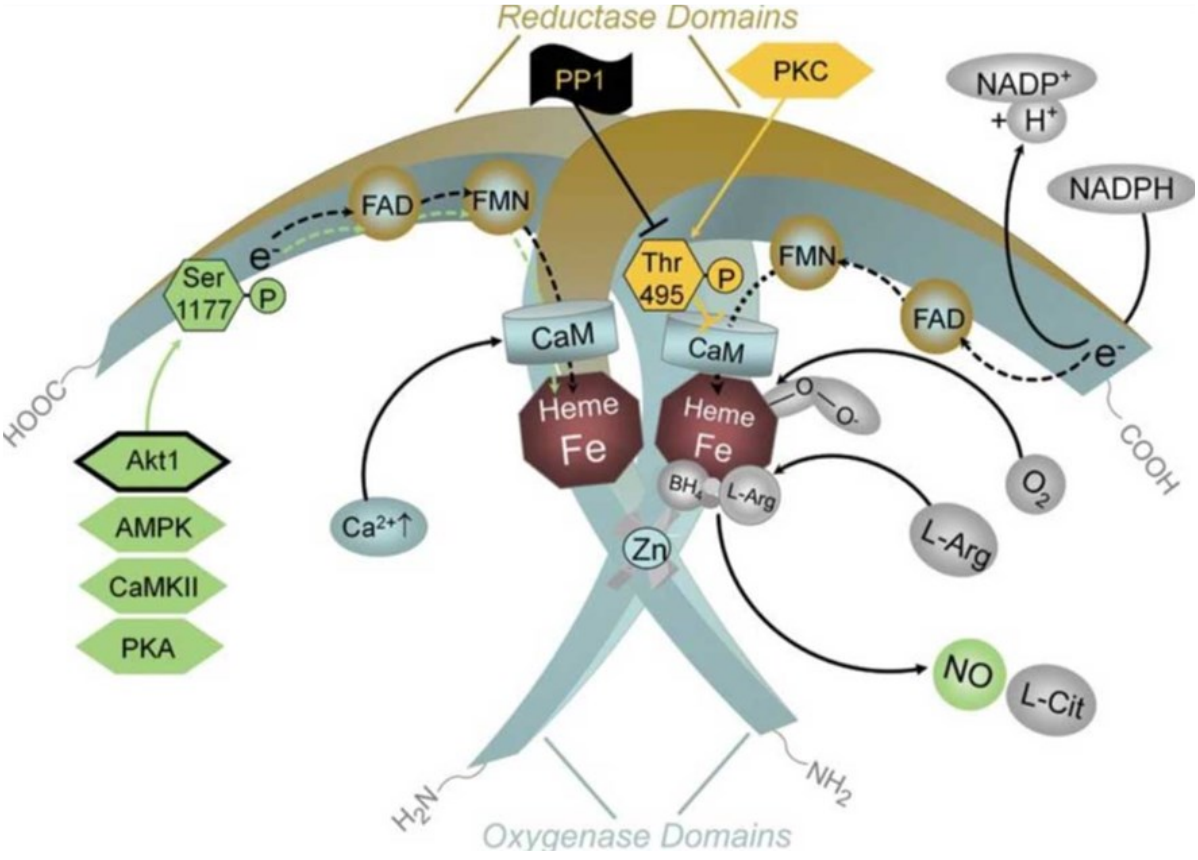

Fig. 1.1 Structure, catalytic mechanism and regulators of NOS enzymes (adapted from Forstermann *et al.*, 2012[3]**.** Schematic showing domains of the Nitric oxide synthase and co-factors that it requires in order to produce NO. Akt kinase (Akt1), AMP-activated protein kinase (AMPK), Ca2+/calmodulin-dependent protein kinase II (CaMKII) and protein kinase A (PKA) are known to phosphorylate S1177, which increases NO production efficiency of NOS isoforms.

1.2 Nitric Oxide Synthases: Localization, Regulation and Function

Neuronal Nitric Oxide Synthase (NOS1): NOS1 is a constitutively expressed in neurons of the central nervous system (CNS). NOS1 contains an amino-terminal PDZ domain, which regulates its sub-cellular localization and activity by mediating interactions with other PDZ domain-containing proteins[16]. Apart from the central nervous system, NOS1 has been detected in spinal cord, adrenal glands, macula densa cells of kidney and in pancreatic islet cells[16,17].

Several studies in the last two decades have reported roles of NOS1 in a variety of synaptic signaling processes. NOS1 has been implicated in vital processes, such as neurogenesis, learning and memory[16]. In the CNS, NOS1 regulates long-term potentiation and long-term inhibition[18,19]. Importantly, retrograde neurotransmission across synaptic junctions is predicted to be involved in memory and engram formation and inhibition of this transmission causes amnesia and hampers learning in animal models[20]. Abnormal NOS1 signaling is presumed to contribute to a variety of neurodegenerative diseases, such as Alzheimer's, Parkinson's and multiple sclerosis[21]. Hyperactivation of NOS1 by massive repeated influx of calcium into neurons is implicated in NMDA receptor mediated neuronal death via excitotoxicity and stroke-like conditions[22].

Inducible Nitric Oxide Synthase/NOS2: NOS2 is usually expressed at very low levels in cells, but as the name suggests, NOS2 expression can be induced by immunostimulatory molecules, such as lipopolysaccharide derived from bacteria and a variety of cytokines[4,9,17]. First identified in macrophages, NOS2 expression can be induced in virtually any cell type

upon treatment with the appropriate immunostimulatory molecules[4]. NOS2 is regulated transcriptionally. Once expressed, it is constitutively active and does not require elevated cytoplasmic calcium levels[3].

NOS2, when induced in immune cells, produces copious amounts of NO, which acts as a major cytotoxic agent in these cells[23]. NO can react with Fe^{2+} bound to proteins and by modifying these iron atoms, NO can modulate activities of key enzymes that utilize Fe^{2+} as a part of their catalytic cycle. These include heme-containing enzymes and iron-sulphur cluster-containing enzymes such as electron transport chain complexes in mitochondria and ribonucleotide reductase[23]. Moreover, the large amounts of NO produced by immune cells can cause DNA damage by base modifications and strand breakage[24]. Such mechanisms are posited as the basis of the cytotoxic and cytostatic effects of NO on microorganisms and tumor cells[25–27]. When induced by appropriate agents, non-immune cells can also express NOS2 and produce large quantities of NO, which can reach neighboring cells and affect their functions[28]. For example, when endothelial cells are induced by cytokines, they can produce NO and kill proximal tumor cells, while induced hepatocytes can produce enough NO to kill malarial parasites resident within[29].

The effect of NO on any cell depends on three main factors - quantity, location and timing. When large quantities of NO are produced by immune cells at the wrong time, in the wrong amount and on the wrong location, it can also harm healthy tissues[30,31]. In animal models, tissue damage is linked to NO or $ONOO^-$ (peroxynitrite) produced by the interaction between NO and superoxide ($O_2^{\cdot-}$) [22]. Most inflammatory and autoimmune lesions have activated,

NOS2-positive macrophages and neutrophils. These activated innate immune cells produce large quantities of NO which can damage surrounding tissue[32].

Neurodegeneration caused by inflammation has been observed in a number of neurodegenerative disorders. We now have some clues about the mechanisms used by activated microglia and astrocytes to kill neurons. Expression of NADPH oxidase and NOS2 in these activated cells generate peroxynitrite, which causes apoptosis in neurons. NO perse can block mitochondrial function by inactivating the electron transport chain and inhibiting cytochrome C, which causes neuronal death[33,34]. Lastly, large quantities of NO produced by NOS2 also play a role in bacterial endotoxin initiated septic shock. The presence of NO causes symptoms like arteriolar vasodilatation, hypotension, and microvascular damage and worsens pathophysiology associated with septic shock[35,36].

Endothelial Nitric Oxide Synthase/NOS3: NOS3 is mostly expressed in endothelial cells. However, recently it has also been shown to be expressed in cardiomyocytes, platelets, human placenta and epithelial cancer cells[17]. In endothelial cells, NOS3 is located in two distinct populations: one in the cholesterol rich domains of the plasma membrane and the other in the Golgi apparatus[37,38]. Targeting of NOS3 to the Golgi and plasma membrane requires co-translational N-myristoylation and post-translational cysteine palmitoylation. Mutation at the Gly2 position, a site for N-myristoylation, inhibits both myristoylation and palmitoylation and NOS3 remains in cytoplasm instead of targeting to membranes[37,39–41]. Mutation of palmitoylation sites Cys15 and Cys26 attenuates plasma membrane targeting but does not affect N-myristoylation and Golgi targeting[39]. In cells, these mutants show reduced NO production when stimulated with pharmacological agents which increase

intracellular calcium, although purified enzyme variants show no differences from wildtype NOS3 in terms of NO production [38,42]. This suggests that acylation of NOS3 and plasma membrane localization or Golgi localization is absolutely required for its activity.

Similar to NOS1, NOS3 also requires calmodulin and elevated cytoplasmic calcium for efficient NO production. Several other proteins are known to interact with NOS3 and modulate its activity. For example, heat shock protein 90 (hsp90) binds NOS3 and serves as an allosteric activator[43,44]. Plasma membrane-associated NOS3 population can interact with caveolin-1, which inhibits the activity of NOS3[44,45]. Caveolin-1 knockout mice show enhanced epithelium-dependent relaxation. Interaction between NOS3 and caveolin-1 could be inhibited by recruitment of calmodulin and hsp90[46].

NOS3 can also be activated by cues that are independent of cytosolic calcium elevation, such as fluid shear stress[47]. Shear stress activates NOS3 by increasing its phosphorylation. NOS3 can be phosphorylated on several of its tyrosine (Tyr), serine (Ser) and threonine (Thr) residues[48,49]. Phosphorylation of Ser 1177 represents an independent and efficient mechanism for NOS3 activation. Phosphorylated Ser1177 increases the flux of electrons from the reductase domain and increases calcium sensitivity of the enzyme[47,48,50]. 17-β-estradiol (E_2) and vascular endothelial growth factor (VEGF) increase NOS3 phosphorylation mainly via Ser/Thr kinase Akt. Insulin activates both Akt and AMP-activated protein kinase. Shear stress increases NOS3 phosphorylation by activating protein kinase A (PKA)[3]. Thus far, Akt is the only regulator of NOS3 which is proven to work in-vivo, because a knock-in mouse carrying phosphomimic mutation Ser1176Asp make NOS3 constitutively active, whereas Ser1176Alan reduces enzyme activity[51]. On the other hand, Thr495 tends to be phosphorylated by protein kinase C (PKC) under non-stimulated

conditions[52]. Phosphorylation of Thr495 is predicted to interfere with calmodulin binding by changing the structure of the calmodulin binding domain. Elevated cytoplasmic calcium and NO production by NOS3 dephosphorylates Thr495 and the dephosphorylation allows better binding to calmodulin[52]. NOS3 also gets phosphorylated at Ser114, Tyr657 and Tyr81. However, mechanisms underlying how these phosphorylation sites modulate NOS3 activity is unclear and is an active area of research[53].

NOS3 is one of the main regulators of numerous vital cardiovascular functions and homeostasis. NO produced by NOS3 acts as a vasodilator for all types of blood vessels by activating soluble guanylyl cyclase (sGC) and increasing cGMP concentrations in smooth muscle cells,[2,54] and NOS3 knockout animals have elevated blood pressure[55]. NO that leaks into the blood vessel lumen inhibits platelet adhesion to the vascular wall and platelet aggregation[56,57]. Such inhibition provides protection against thrombosis. It also decreases the platelet-derived growth factors (PDGF), thereby inhibiting smooth muscle proliferation. Thus, NOS3 shapes vascular remodeling to adapt to chronic changes in flow[58]. By preventing platelet aggregation and PDGF release, NO also prevents fibrous plaque formation, which is a critical step in atherogenesis. It thus acts as an anti-atherosclerotic agent[59]. Additionally, decreased NO production from endothelial cells has been shown to be associated with a number of cardiovascular diseases.

NO produced by NOS3 also regulates postnatal angiogenesis by acting as a messenger downstream of angiogenic factor signaling. Mice deficient for NOS3 also show impaired neovascularization[60]. Recent findings in mice lacking NOS3 showed NO is important for

fetal lung development. The lung phenotypes observed in these mice are similar to those observed in alveolar capillary dysplasia which causes hypertension in newborns confirming the role of NO in angeiogenesis[60]. NOS3 is critical for angiogenesis post-ischemia as it mobilizes endothelial progenitor cells[61]. Mobilization of endothelial progenitor cells by VEGF is reduced in mice lacking NOS3. In a model of hind-limb ischemia in NOS3 knockout mice, intravenous infusion of wild-type progenitor cells can rescue the defective neovascularization, but it does not work with bone marrow transplantation. This suggests that mobilization of progenitor cells from the bone marrow is impaired in NOS3 knockout mice. Indeed, matrix metalloproteinase family member 9, which is required for stem cell mobilization, was reduced in the bone marrow of these mice. Reduced systemic NO bioactivity seen in ischemic heart disease may therefore contribute to impaired neovascularization[62].

NOS3 and cancer

Involvement in cell cycle regulation, apoptosis and angiogenesis is in line with its dichotomous roles in the maintenance of cancer and tumorigenesis[25,31,63]. NO plays broad roles when it comes to cancer growth. It regulates cellular transformation, size of neoplastic lesions, and initiation of metastatic cascade. NO also mediates genotoxic effects, such as DNA lesion by formation of mutagenic species, by directly modifying DNA or by inhibiting DNA repair mechanisms. NO can also cause double strand breaks and G to A mutations[24,64–66].

In cancer cells, NO inhibits caspase activity by S-nitrosylating critical cysteine residues and provides efficient means to block apoptosis. Other means by which NO blocks apoptosis

involve direct or cGMP-mediated inhibition of cytochrome C release, overexpression of Bcl-2 which controls the mitochondrial permeability, increased expression of Hsp70 and Hsp32, and activation of cyclooxygenase-2[67]. NO also controls tumorigenesis by regulating angiogenesis. NOS3-generated NO provides increased blood flow to tumors via dilation of surrounding vessels. It decreases interactions between endothelial cells and leukocytes and increases vascular permeability[68]. VEGF released by tumor cells requires functional NO and sGC pathways in the target cell to promote the growth of new blood vessels. NO directly activates COX-2 which in turn stimulates the production of prostaglandins and other pro-angiogenic growth factors. NO also mediates metastasis by overexpression and activation of matrix metalloproteinase family proteins MMP-2 and MMP-9 and downregulation of MMP antagonists such as TIMP-2 and TIMP-3[69]. Tumor-derived NO inhibits proliferation of leukocytes thereby, downregulating the anti-tumor immune responses[24].

The role of NO in tumorigenesis and tumor maintenance has been extensively investigated for epithelial cancers[70,71]. NO has been shown to play a role in the growth of pancreatic carcinoma and breast cancers. Overexpression of NOS2 and NOS3 has been reported in breast cancer tissues and in breast carcinoma cell lines. Moreover, this expression correlates with tumor grade and cancer stage. Increase in NOS activity has been observed in aggressive breast cancers as compared to benign or normal breast tissue[72,73]. Elevated levels of NO and its metabolites have also been detected in the blood samples of breast cancer patients. Jadeski et al. showed that the presence of NOS3 in breast metaplastic cells promotes the transformation of metaplastic epithelium into carcinoma[74]. NOS3-derived NO increases blood flow towards tumors and also facilitates angiogenesis. This explains the positive correlation between NOS3 levels, NO biosynthesis and grade of malignancy[73]. Levels of

nitrotyrosine, a proxy for NO production, correlate with VEGF-C expression and lymph node metastasis in breast cancer[75].

Steroid hormones greatly influence breast cancer growth. Both estrogen and progesterone regulate expression of NOS isoforms and tumor cell homeostasis in breast carcinomas[76,77]. NOS3 expression has been found to correlate with estrogen receptor expression in human breast cancer cell lines[78]. Progesterone on the other hand increases NOS2 expression. NO produced by NOS3 mediates the proliferative effects of estrogen, whereas high levels of NO produced by NOS2 are associated with increased apoptosis upon progesterone treatment[79,80]. Amount, location and duration of NO production could give rise to different physiological outcomes. Thus, measuring activities of NOS isoforms could lead to better understanding of these opposing effects and pave a way towards development of better cancer therapies.

1.3 State of the art technologies to detect NOS activity and their limitations

I have thus far laid the basis for the need for reliable measurements of NO or NOS activity with sub-cellular resolution in order to understand biological outcomes. However, there are number of challenges to achieve this goal. Low concentrations of endogenous NO and its short half-life are the major hurdles[81]. In cells, NOS1 and NOS3 produce nanomolar concentrations of NO, while NOS2 can produce micromolar concentrations. Another complication is that after it is generated by a NOS isoform, NO diffuses rapidly from the point source and reacts with biomolecules in its path. For example, NO directly reacts with cysteine and tyrosine residues on proteins and modulates the protein functions (Discussed in Chapter 4 section 4.1). NO can also be scavenged by electron-rich centers such as heme and

iron-sulphur clusters, or by oxidation with oxygen and endogenous ROS to form nitrate and nitrite. As a consequence of these reactions, NO has a half-life of milliseconds to 7 seconds under physiological conditions[82]. While there are several techniques that can measure NO from bulk tissue extracts, very few can be employed to measure NO production in single cells.

Histochemistry and fluorescence in-situ hybridization of NOS isoforms provide high sensitivity and selectivity but are only able to provide information on presence and sub-cellular distribution without yielding enzyme activity or absolute NO levels. Other detection methods which can report directly on NO or NO metabolite are chemiluminescence, electron paramagnetic resonance based spectroscopy, electrode-based sensors, small molecule fluorophores and recently, genetically encodable NO sensitive fluorescent proteins[81,83]. Chemiluminescence requires reaction with cytotoxic agents like ozone while EPR has overall lower spatial resolution making these techniques face limitations when it comes to live single cell measurements[84,85]. Both small molecule and protein-based fluorescence sensors are the current state-of-the-art and most widely used assays for single cell NO measurements. I will discuss two such fluorescence-based NO sensing technologies which are available commercially and used widely. i) 4,5-Diaminofluorescein, a small molecule fluorophore whose fluorescence increases upon reaction with NO and ii) geNOps, a genetically encodable fluorescent protein-based NO sensor whose fluorescence decreases upon reaction with NO.

4,5-Diaminoflurescein (DAF) was synthesized and validated as an NO sensor by Nagano's group in 1998[86,87]. DAF has electron-donating groups such as amines attached to benzoic ring of a fluorescein core. In this form, photo-induced electron transfer (PeT) from the aromatic diamino group quenches its fluorescence. Upon reacting stoichiometrically with

NO and O_2, DAF forms DAF-triazole and this disrupts PeT, which restores fluorescence (Fig. 1.2)[86]. The high-fold-change and its ease of use have been exploited in many fluorescence microscopy, cell sorting and fluorimetric studies[81,88,89]. DAF provides excellent signal-to-noise ratio, high selectivity, high sensitivity and desirable photophysical properties by tolerating change in the fluorophore core. The only major disadvantage DAF faces is rapid intracellular and intercellular diffusion after reaction with NO, which blurs out spatial information and gives average readout of NOS activity.

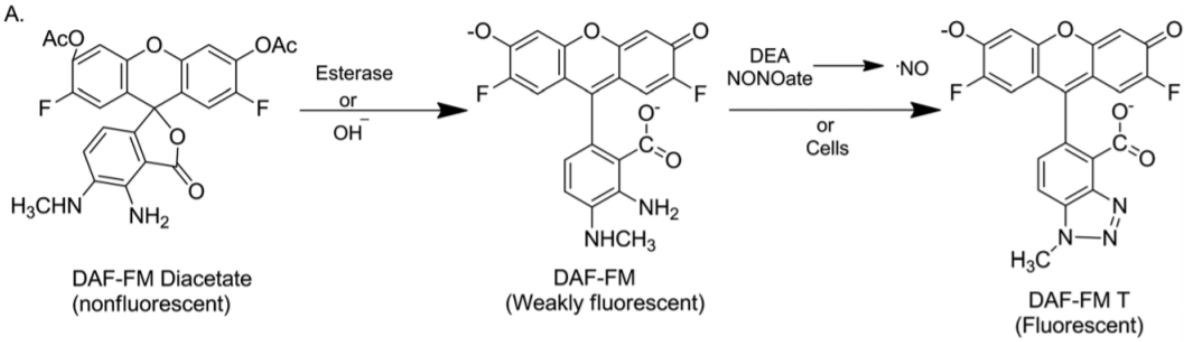

Fig. 1.2 NO sensing by DAF-2DA (adapted from Mainz et al., 2012)[90]. Cell permeable molecule DAF-FM Diacetate enters cells and gets processed by cytoplasmic esterase to DAF-FM, which upon reaction with NO forms DAF-triazole.

Genetically encodable NO probes (geNOps) were developed by the Malli group in 2016[91]. These probes contain different fluorescent proteins directly conjugated to an iron-containing bacterial NO-binding domain. The NO binding domain brings NO in close proximity of the fluorophore which is presumed to affect electron density in the vicinity, thereby quenching the fluorescence (Fig. 1.3). geNOps is quasi-reversible, its fluorescence recovers when NO dissociates from the NO-binding domain, which allows for dynamic imaging of NO[83,91]. Being genetically encodable, geNOps can be targeted to various sub-cellular locations and

provide single-cell as well as sub-cellular NO levels. However, geNOps is limited by its low, negative fold-change in signal which precludes real-time long-term imaging as photobleaching would also affect the signal. Most fluorescent proteins are pH sensitive, and this restricts use of geNOps to those regions where pH is near neutral. geNOps cannot be used in organelles with acidic pH e.g. endosomes, Golgi or phagosomes. Its iron center in the NO binding domain cannot acquire iron from the cytoplasm and requires addition of millimolar quantities of iron which would affect cell physiology. The iron-containing NO binding domain is also sensitive to ROS, such as H_2O_2, and its fluorescence is quenched[91]. This cross reactivity to ROS gives false positive signals and thus it cannot be used in environments with high ROS levels, such as phagosomes.

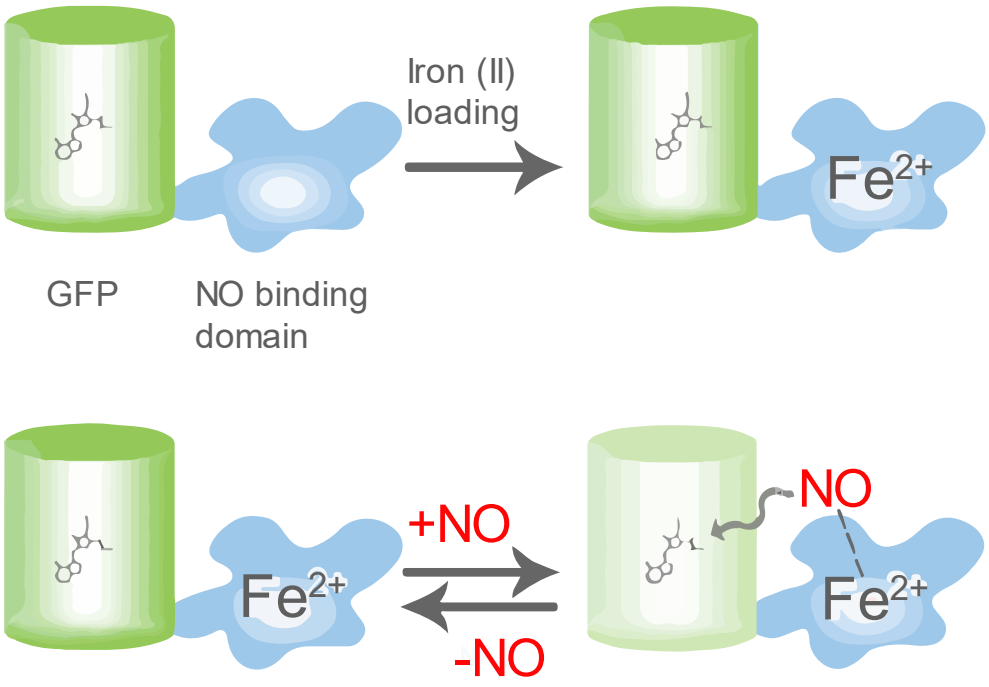

Fig. 1.3 NO sensing by geNOps (adapted from Eroglu et al., 2018)[83]. geNOps is a fusion protein of GFP and NO binding domain. Iron center of NO binding domain can form coordination bond with Fe^{2+} which changes electron density around the GFP and quenches its fluorescence.

1.4 DNA-based ratiometric sensors for small molecules and ions in Biological systems.

To quantitatively measure activities of sub-cellular NOS3 populations, we require a sensor that is selective, targetable, pH-insensitive and preferably ratiometric. In short, we required a sensor which combines the selectivity and photophysical properties of small molecule sensors with sub-cellular targeting available to proteins. We therefore chose a DNA-based sensor, which combines these properties and has been used *in-cellulo* and *in-vivo* for quantitative measurements of positively charged ions (H^+ and Ca^{2+}), negatively charged ions (Cl^-), reactive species (HOCl and NO) and small molecule second messengers (cAMP)[92–101].

DNA-based sensors are ratiometric, here a strand containing a sensing fluorophore is hybridized with an equimolar concentration of a strand containing the reference fluorophore. The reference fluorophore is not sensitive to the environment and hence can be used for normalizing purposes, just as a loading control on a western blot and also as a fiducial marker to track the sensor in case the sensing fluorophore is dim to start with. Ratiometric imaging (Sensor fluorophore/reference fluorophore) corrects for sensor intensity differences inside cells which might arise due to cell-to-cell heterogeneity, trafficking differences and non-uniform probe uptake, that all results in inhomogenous probe distribution.

DNA nanodevices are modular and programmable, which allows for accommodation of multiple functionalities on a single device. These functionalities include sensing fluorophores for simultaneous sensing of multiple analytes, normalizing fluorophores, targeting moieties and immunogenic signals[102]. DNA nanodevices are very much plug-and-play technology as their modularity offers the capabilities to re-use pre-characterized

functionalities on newer sensors or combining already known sensors onto a single device[96,101,103].

Taking advantage of these properties, we designed DNA-based NO-sensitive probes, called NOckout to measure NOS3 activity[104]. NOckout combines the selective chemistry and photostability of small molecule NO probes as well as offers stable spatial localization afforded by protein sensors. These probes are modular, ratiometric, pH insensitive and sub-cellularly targetable, making them well suited to quantify activities of NOS3 sub-populations.

1.5 Scope of this thesis

Despite the clear importance of both NOS sub-populations, it has been challenging to delineate the contribution of either pool in terms of their NO contribution or physiological relevance. In this thesis we will discuss how we attempted to answer some of these questions.

Chapter 2 will discuss the design and characterization of NOckout probes followed by benchmarking of our probe with state-of-the-art NO probes.

Chapter 3 will discuss and compare NO production of plasma membrane-associated NOS3 versus that of Golgi-associated NOS3, followed by an attempt to dissect the mechanism responsible for the apparent differences in activities of these NOS3 populations.

Chapter 4 discusses a potential role of one NOS3 in the maintenance of Golgi morphology, and potential molecular players involved in this process.

Chapter 2

Design, Characterization and *in-cellulo* performance of NOckout devices

2.1 Introduction: Design and Assembly of NOckout

Most approaches to detect NOS activity are based on NO-sensitive small molecule fluorophores (Chapter 1)[86,105,106]. However, after reacting with NO diffuse these fluorophores rapidly throughout the cytoplasm and to the extracellular space, thereby blurring the spatial information of NO production. Recently developed genetically encodable probes offer the necessary spatial information but they are also sensitive to pH and ROS[91]. This restricts the use of such probes mainly to the cytoplasm with less applicability to other organelles such as late endosomes, lysosomes, Golgi-Apparatus, mitochondria etc. Genetically expressed NO sensors also require supplementation of millimolar levels of Fe^{2+} to function which impedes their use *in-vivo*[91]. To measure activities of NOS3 populations in cells, we need a probe with the high specificity and photostability afforded by small molecules, while retaining the spatial information associated with protein probes. We developed DNA-based probes denoted NOckout, that provides quantitative information about sub-cellular NOS3 activity using ratiometric imaging. We made two NOckout variants, NOckout^{PM} and NOckout^{TGN} to quantitatively image NO with sub-cellular resolution, NOckout includes the following modules with stoichiometric precision integrated into a single probe,

(i) an NO-sensitive small molecule fluorophore which is specific, photostable and works over a wide range of pH values. This fluorophore should also be able to sense a range of NO concentrations encountered inside cells and with response kinetics fast enough to capture NO

molecules before they react with their biological targets[81]. For this purpose, we chose an NO-sensing fluorophore based on the diaminorhodamine fluorophore DAR (Fig. 2.1)[105]. Fluorescence of DAR is quenched by intramolecular photoinduced electron transfer arising from the aromatic diamino group (OFF state, Fig. 2.1). DAR reacts stoichiometrically with NO and its auto-oxidized form (N_2O_3) to form the triazole derivative DAR-T[87], which disrupts photoinduced electron transfer, thereby turning on fluorescence (ON state, Fig. 2.1), with $\lambda_{ex} = 550$ nm and $\lambda_{em} = 575$ nm (ex- excitation and em- emission). DAR-T offers high photostability, brightness ($\phi = 0.42$, $\varepsilon = 76{,}000\ M^{-1}\ cm^{-1}$), pH insensitivity from pH 4–10 and has an NO detection limit of ~7 nM[105].

(ii) an internal reference fluorophore for ratiometric quantification. This reference fluorophore corrects for DAR intensity differences inside cells which might arise due to cell-to-cell heterogeneity, trafficking differences and non-uniform probe uptake. We used different reference dyes for each NOckout variant, NOckout^{PM}, a variant targeted to the plasma membrane uses Alexa fluor 488 (Alexa488) as the normalizing fluorophore, whereas NOckout^{TGN}, a variant targeted to Golgi, uses Alexa fluor 647 (Alexa647) as the normalizing fluorophore. Alexa488 and Alexa647 were chosen because of their high photostability, brightness and insensitivity to pH, ROS and other analytes that NOckout might encounter inside cells[98,107]. These spectrally distinct reference fluorophores enable simultaneous tracking and visualization of both NOckout variants in duly labeled cells.

(iii) a targeting module to stably localize NOckout either at the Golgi or at the plasma membrane. NOS3 is known to localize to cholesterol rich domains on the plasma membrane. Thus, NOckout^{PM} was covalently conjugated to triethylene glycole-Cholesterol (TEG-Cholesterol). Upon encountering the plasma membrane, the cholesterol moiety inserts into the outer leaflet of plasma

membrane and stably localizes NOckout^{PM} onto the plasma membrane[108,109]. NOckout^{PM} localization is ideal because the cholesterol moiety is expected to position it in close proximity of NOS3 on the opposite face of the plasma membrane. NOckout^{TGN} on the other hand uses a very high affinity DNA-aptamer (5-TRG2, K_d – 18 nM) that binds hypo-glycosylated MUC1 on the plasma membrane of epithelial cancer cells[110]. Upon incubation with NOckout^{TGN}, the MUC1 aptamer 5-TRG2 engages hypo-glycosylated MUC1 on the plasma membrane and labels the lumen of the trans-Golgi network (TGN). MUC1 traffics back to the Golgi through retrograde endocytosis and ferries NOckout^{TGN} along with it. In this chapter, I describe the design, synthesis, *in-vitro* and *in-cellulo* characterization of these NOckout devices.

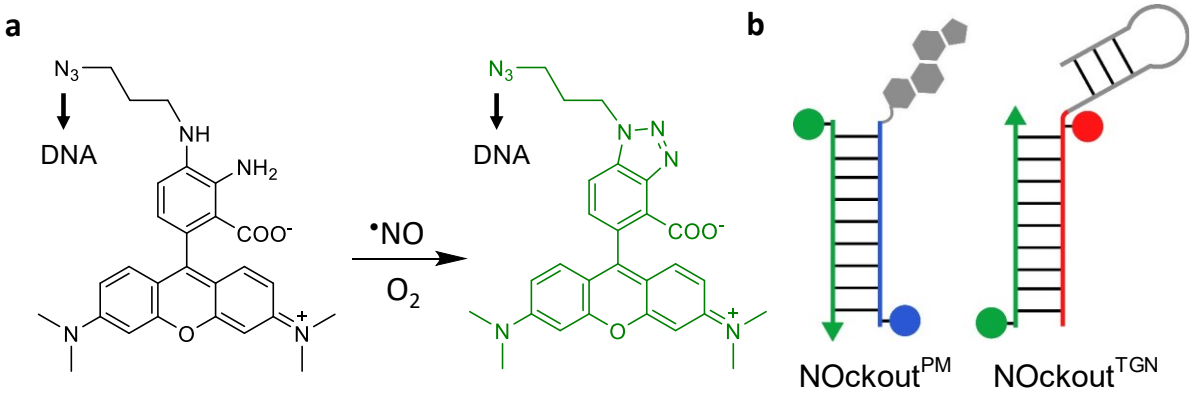

Fig. 2.1 Design of NOckout probes. **a**, DAR structure and mechanism of NO sensing, with arrows showing the site of DNA conjugation. **b**, Design of two NOckout reporters, NOckout^{PM} (plasma membrane-targeting) and NOckout^{TGN} (Golgi-targeting). Green and blue filled circles in NOckout^{PM} denotes sensing dye (DAR) and normalizing dye (Alexa488), respectively. In the case of NOckout^{TGN}, Alexa647 (red filled circle) functions as the normalizing dye. Cholesterol moiety (gray) conjugated to the NOckout^{PM} sensor targets it to the plasma membrane and 5TRG2 aptamer (gray hairpin) conjugated in NOckout^{TGN} ferries it to the Golgi.

2. 2 Materials and Methods

Reagents

Oligonucleotides (Supplementary Table 1) were purchased from Integrated DNA Technology (IDT, USA). HPLC purified oligonucleotides were ethanol precipitated before using them for NOckout assembly. DAR was functionalized to S1 (Scheme 1). Oligos were quantified using UV-visible spectrophotometry (Shimadzu UV-2700) and were dissolved in de-ionized water to prepare a 200 µM stock, aliquoted and stored at −20 °C until used.

Small molecules such as 1400W, PTIO, 17-β-estradiol (E_2), L-NAME and DEA-NONOate were purchased from Cayman chemicals. All other chemicals used for the DAR-synthesis were purchased from Sigma Aldrich. Methylene blue and PTIO stock solutions were prepared in DMSO (50 mM). Whereas, E_2 stock solution was prepared in ethanol (10 mM), DEA-NONOate stocks were prepared in NaOH (10 mM, pH 9), and were all used within a week. For incubations lasting longer than 24 h, the aforementioned small molecules were replenished to the same concentration in new medium every 24 h.

Name	Sequence
S1	5′- /5AzideN/ATC AAC ACT GCA CAC CAG ACA GCA -3′
$S2^{PM}$	5′- /5Alex488N/TGC TGT CTG GTG TGC AGT GTT GAT /3CholTEG/ -3′
$S2^{TGN}$	5′- GGC TAT AGC ACA TGG GTA AAA CGA CTT TGC T/iAlexa647N/G TCT GGT GTG CAG TGT TGA T -3′

Table 1: Sequences of chemically modified oligonucleotides used in the study.

DsiRNA used for the knockdown of NOS3 were purchased from Integrated DNA Technology (hs.Ri.NOS3.13.1 and hs.Ri.NOS3.13.2), NOS3 forward primer: AGC GGC TCC CAG GCC

CAC GA, reverse primer: CAG ACC TGC AGT CCC GGG CA and β-actin forward primer: CCT CGC CTT TGC CGA TCC, reverse primer: GAG TCC ATC ACG ATC CCA GT.

NOckout sensor assembly (Scheme 1**)**

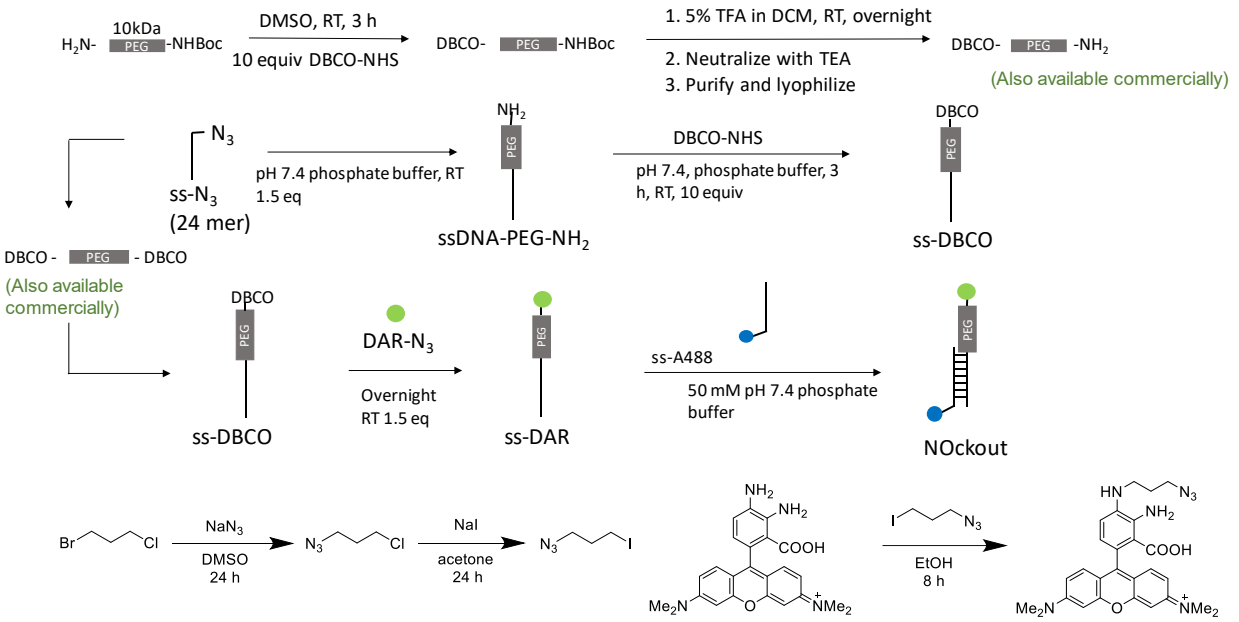

Scheme 1: Stepwise synthesis of DAR-S1 strand and assembly of NOckout. Where ss-DAR is S1 conjugated to Diaminorhodamine and ss-A488 is S2.

PEG in between S1 and DAR prevents PeT which has been observed when rhodamine fluorophores are conjugated to oligonucleotides[111]. Attachment of DAR directly to DNA in the absence of PEG brought down maximum *in vitro* fold change of NOckout to 2-fold as compared to 6-fold when PEG is present (Dr. Aneesh T. Veetil's Unpublished data).

Synthetic procedures

1-azido-3-iodopropane (**Scheme 1**) was synthesized using 1-bromo-3-chloropropane as precursor following procedure described by Yao et al.[112]. DAR-4M was synthesized following synthetic procedures from to Kojima et al.[105].

For synthesis of DAR-N_3, DAR-4M (28mg, 0.067 mmol) was heated in dry ethanol until it starts refluxing then add 1-azido-3-iodopropane (25 mg, 0.12 mmol) every two hours. Reaction was monitored by LC-MS. Reaction was stopped once maximum monoalkylated product was detected on LC-MS. Then, crude product was purified by chromatography with MeOH/DCM (1:9 v/v) as a mobile phase to isolate DAR-N_3 (2.7 mg, 8%). Unreacted DAR-4M was recovered from the plate.

DAR-N_3 NMR peaks: ^{1}H NMR(CDCl3, 500 MHz, ppm) δ = 1.98 (m, 2H), 2.97 (s, 12H), 3.27 (t, 2H, J = 6.5 Hz), 3.52 (t, 2H, J = 6.5 Hz), 6.41 (dd, 2H, J = 2.5 Hz, 8.5 Hz), 6.43 (d, 1H, J = 3.0 Hz), 6.47 (d, 2H, J = 2.5 Hz), 6.76 (d, 2H, J = 4.0 Hz), 6.85 (d, 1H, J = 8.0 Hz);

^{13}C NMR (CDCl3125 MHz, ppm) δ = 33.0, 40.5, 42.2, 49.7, 98.6, 108.5, 108.8, 111.9, 113.3, 118.1, 129.2, 135.7, 135.9, 152.2, 153.2, 171.4

1. **Conjugation of the dibenzocyclooctyne (DBCO) group:** Mono-protected amine functionalized 10 kDa polyethyleneglycol (3 mg, Boc-NH-PEG-NH_2, Creative PEG works) was dissolved in 150 µl of dry DMSO. To make assay system basic (higher pH), 2 µl of triethylamine was added. DBCO-NHS ester (Sigma-Aldrich) was added to the reaction at a final concentration of 20 mM, stir reaction mixture at room temperature for 3 hours. The reaction mixture was diluted 100 times with de-ionized water to bring down DMSO content to less than 1%. Unreacted DBCO-NHS ester was removed from reaction mixture by centrifugation using 3 kDa Amicon cut-off filters, presence of remaining DBCO-NHS ester by UV-Vis spectrophotometer of each Amicon flow through. This purification step was repeated until there was no detectable absorbance at 309 nm in the

Amicon flow through. Purified DBCO-PEG product was lyophilized and can be stored at −80 °C up to 3 months.

2. **Deprotection of *tert*-butyl carbamate (Boc):** Dissolve 5 mg of DBCO-PEG in 200 µl trifluoroacetic acid/dichloromethane (5:95 v/v). Stir reaction mixture overnight at room temperature. Evaporate solvent using a gentle nitrogen flow. Add 100 µl de-ionized water and neutralized mixture with triethylamine. The product concentration was determined by UV spectrophotometer (λ_{ex} = 309 nm). This deprotected PEG derivative was lyophilized and can be stored at −80 °C up to 3 months.
3. **DNA-PEG conjugation:** 50 µM of 24-mer ssDNA with a 5′-azide modification (strand S1, see Table 1 for sequence) was dissolved in 50 mM potassium phosphate buffer, pH 7.4. Add 75 µM deprotected PEG derivative and stir the reaction mixture for 12 hours. Reaction progress was checked by gel mobility shift assay on a 15% PAGE. PEG conjugated DNA migrates much slower than 24-mer DNA without the PEG. Conjugated product was purified by 10 kDa molecular weight cut-off Amicon centrifugation using 100 mM phosphate buffer, pH 7.4 as exchange buffer.
4. **PEG-DNA-DAR conjugation:** DAR-N_3 was dissolved in DMSO to to make a stock solution of 3 mM. Exact concentration was determined by UV spectrophotometer (λ_{ex} = 571 nm, $\varepsilon = 7.8 \times 10^4$ M cm^{-1}). 1.5 equivalence of DAR-N_3 was added to PEG-S1. Stir reaction mixture at room temperature for 12 hours, purify PEG-DNA-DAR (ssDAR or DAR-S1) using 3 kDa cut-off Amicon centrifugation using 100 mM phosphate buffer pH 7.4, as exchange buffer. Flow through from Amicon was checked by UV spectrophotometer and this step was repeated until absorbance from DAR-N_3 was undetactable.

5. **Annealing:** DAR-S1 and $S2^{PM}$ or $S2^{TGN}$ (Table 1) were mixed in equimolar ratios to a final concentration of 10 μM in 20 mM potassium phosphate buffer (pH 7.4) supplemented with 100 mM KCl. Strands were annealed by heating mixture to 90 °C and decrease temperature with a rate of 5 °C per 15 min until it reaches room temperature, equilibrate sample at 4 °C overnight.

Assembly of NOckout was confirmed by a gel mobility shift assay using 15% native PAGE (running buffer- 1× TBE, 100 V constant voltage for 120 min at RT). PAGE was imaged using Bio-Rad ChemiDoc MP imaging system (Fig. 2.2). Alexa488 (referred to as 'B') channel images for gel were acquired using Epi-blue filters ($\lambda_{ex.}$ 460–490 nm and λ_{em} 518–446 nm). DAR channel images for gel (referred to as 'G') were acquired using Epi-green filters ($\lambda_{ex.}$ 520–545 nm and $\lambda_{em.}$ 577–613 nm). Alexa647 channel images for gel (referred to as 'R') were acquired using Epi-red filters ($\lambda_{ex.}$ 625–650 nm and $\lambda_{ex.}$ 675–725 nm). The gel was then stained with Ethidium Bromide solution for 5 min and imaged in EtBr channel. Due to very broad excitation and emission filters in ChemiDoc MP gel imager, there is a bleed through of Alexa488 channel into the Epi-green filter set (asterisk, DAR channel), as observed in the gel (Fig. 2.2). Note that these filer sets are used only while imaging the gel for NOckout assembly; microscope imaging was done using specific narrow filter sets as mentioned in the Image acquisition section and these two are in no way related.

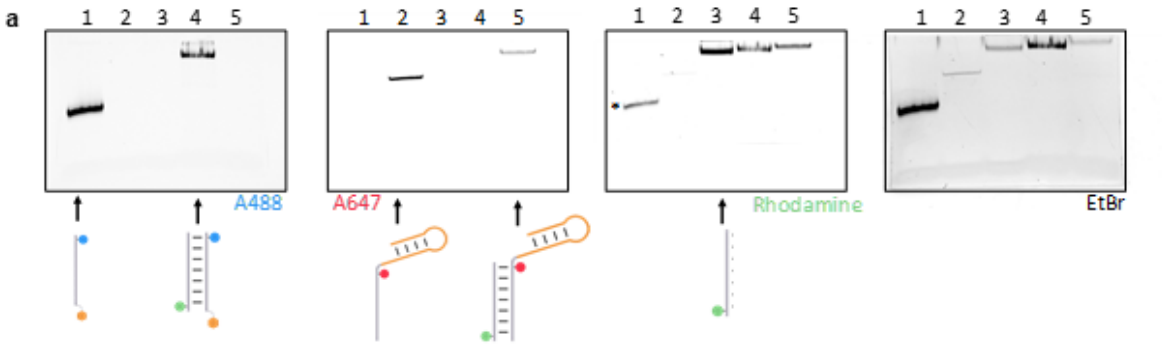

Figure 2.2: **Assembly of NOckout probes. (a)** 15% native PAGE showing assembly of NOckout probes. Lane 1: Strand 2^{PM}, Lane 2: Strand 2^{TGN}, Lane 3: DAR-PEG-S1, Lane 4: NOckout^{PM} and Lane 5: NOckout^{TGN}.

In-vitro fluorescence measurement

All fluorescence spectra present in this thesis were acquired using Fluoromax-4 (Horiba Scientific, USA) spectrophotometer. Stock of NOckout sensors was diluted to achieve 100 nM final concentration with 100 mM sodium phosphate buffer, pH 6.0, unless specified otherwise. DAR, A488 and A647 emission spectra were recorded by exciting the samples at 550 nm, 488 nm and 650 nm, respectively (Fig. 2.3). Emission spectra were collected for the range 560–620 nm (DAR), 495–540 nm (Alexa488) and 655–700 nm (Alexa647). DEA-NONOate (Cayman, USA) was added to sample at a final concentration of 50 µM. The samples were placed back onto the spectrometer as soon as possible and emission spectra of DAR was recorded with time interval of 30 s. Alexa488 or Alexa647 spectra were recorded before the addition of DEA-NONOate and 3.5 min after it. Emission intensity of DAR either at 571 nm (before addition of $NO^{\cdot}$ donor) or at 578 nm (after the addition of NO donor). DAR (G) intensity was normalized to that of Alexa488 emission intensity at 520 nm (B) or to that of Alexa647 emission intensity at 660 nm (R). Fold change in G/B or G/R ratio was calculated from the ratio of steady-state G/B or G/R values after to before NO donor addition. To assess pH sensitivity, stocks of NOckout sensors were diluted in

100 mM sodium phosphate buffer pH 6.0 or 100 mM sodium phosphate buffer pH 7.4 before the start of experiment (Fig. 2.3e). Fluorescence spectra were acquired before the addition of DEA-NONOate and 15 min after it as described above.

Cell culture

Breast cancer epithelial cancer cell lines T-47D and MCF-7 were kind gifts from Prof. Geoffrey Greene (The Ben May Department for Cancer Research, The University of Chicago). Breast epithelial cell lines derived from healthy individuals, MCF-10A and 184A1, were kind gifts from Prof. Marsha Rosner (The Ben May Department for Cancer Research, The University of Chicago). The cells were cultured following the ATCC guidelines. Briefly, T-47D cells were grown in RPMI-1640 (Life technologies, USA), This medium was supplemented with 100 U/ml of penicillin, 100 µg/ml of streptomycin (Life Technologies, USA), 10% final concentration of heat inactivated FBS (Life Technologies, USA) and 0.2 U/ml human insulin. MCF-7 cells were grown in DMEM/F-12 1:1 supplemented with 100 U/ml of penicillin, 100 µg/ml of streptomycin, 10% final concentration of heat inactivated FBS (Life Technologies, USA) and 0.01 mg/ml of human insulin. MCF-10A and 184A1 cells were grown in MEBM + MEGM (ATCC, USA) medium containing 0.005 mg/ml transferrin and 1 ng/ml cholera toxin. Cells were maintained at 37 °C at 5% CO_2 concentration in a humidified water-jacketed incubator. All the experiments described in this thesis were performed at early passage number (after receiving, $n < 17$) and no later than 80% confluency.

Immunofluorescence staining

T-47D and MCF-7 were cultured on a glass bottom (10 mm diameter) 3.5 cm imaging dish until they reach 60% confluency. Cells were treated with small molecule NO scavengers (20 μM methylene blue, 20 μM hemoglobin and 100 μM PTIO), NOS2 inhibitor (10 μM 1400W) or small molecule ROS scavenger (2 mM TEMPOL). After the treatment, cells were washed three times with 1× PBS (pH 7.4) and were fixed by paraformaldehyde, final concentration 4% for 15 minutes at room temperature. Subsequently, cells were permeabilized using triton X-100 (final concentration 0.25%) followed by blocking using BSA (3% final concentration in 1× PBS). Cells were then incubated with monoclonal or polyclonal primary antibodie(s): mouse monoclonal anti-eNOS antibody (SantaCruz Cat# sc-376751), Rabbit Polyclonal anti-*S*-nitrosocysteine antibody (Abcam Cat# ab94930 or Abcam Cat# ab50185), Rabbit polyclonal anti-Giantin antibody (Abcam Cat# ab24586) or Mouse monoclonal Anti-GM130 antibody (BD Biosci. Cat# 610822). These antibodies were diluted in blocking buffer (3% BSA in 1× PBS) and incubated with cells for 1 hour at room temperature. Cells were subsequently washed with 1× PBS (3 times, 5 min each wash). Cells were incubated with respective secondary antibodies conjugated with either Alexa488 or Alexa647 (diluted in blocking buffer) for 1 h at room temperature. Cells were washed with 1× PBS for 5 min each (3×) to remove excess secondary antibody. 5 μM Hoechst 33342 was added to stain nuclear DNA for 10 min just before imaging. Images of stained cells were acquired using Leica SP8 laser scanning confocal microscope using excitation wavelengths of 405 nm for Hoechst, 488 nm for Alexa488 and 647 nm for Alexa647. Images were processed using Fiji/Image J and maximum *z* stack projection of 2–3 *z*-planes were used in representative images.

Image acquisition

T-47D were cultured on glass-bottom imaging dishes as mentioned above in the cell culture section. Cells were washed two times with Hank's balanced salt solution (HBSS, pH 7.4) before incubating them with 500 nM NOckout^{PM} for 10 min or with 500 nM NOckout^{TGN} for 30 min at 37 °C in a CO_2 incubator. After the incubation cells were washed three times with HBSS to remove any excess probe. While acquiring steady-state images (Fig. 2.8), cells were treated with indicated small molecule inhibitor or donor for 1 h in complete RPMI-1640 medium. To avoid cytotoxicity, care was taken not to exceed the final concentration of DMSO >1% at any point of the experiment. As a negative control, 1% DMSO was used in untreated (Basal) cells. Since DEA-NONOate is cell impermeable, it works well with experiments involving NOckout^{PM}. It is straightforward to add it to the cells to fully turn on the NOckout^{PM} at the plasma membrane. On the contrary, for the TGN, we incubated NOckout^{TGN} beforehand with DEA-NONOate in-vitro, fully turned it on and then pulsed cells with the turned-on NOckout^{TGN} (500 nM). Then the cells were washed and imaged (Fig. 2.8).

For simultaneous pulsing of NOckout devices, cells were treated with 500 nM NOckout^{TGN} for 30 min and in the last 10 min cells were co-incubated with 500 nM NOckout^{PM}. To get a bleaching profile or to achieve the lowest signal, cells were treated with 500 µM PTIO 15 min before the NOckout pulse. Images were acquired on a laser scanning confocal Leica SP8 microscope using a 63x 1.4 numerical aperture UV objective. Desired excitation and emission wavelengths were achieved using a white light laser along with notch and acousto-optical tunable filters. Fluorophores were imaged using following settings: Alexa488 (λ_{ex} = 488 nm, λ_{em} = 500–540 nm), DAR (λ_{ex} = 554 nm, λ_{em} = 565–610 nm) and Alexa647 (λ_{ex} = 647 nm, λ_{em} = 665–710 nm).

Image analysis

Image analysis was carried out using Image J/Fiji[113]. Mean auto-fluorescence intensity was subtracted from images before ratiometric analysis. For representation, images were further processed by smooth and noise reduction despeckle functions. To represent heatmap G/B or G/R images, a mask for each normalizing fluorophore channel was constructed using Otsu thresholding then these images were multiplied with both channels of the image, the mask-multiplied images were used for division. The ROI were selected using normalizing channel to select either TGN (Alexa647 channel) or plasma membrane (Alexa488 channel), later these regions of interest (ROIs) were recalled in the DAR channel to measure intensity in all three channels. These raw values were used to plot G/B or G/R values in using Origin Lab (Fig. 2.8).

***In-vitro* specificity assay for NOckout**

Fluorescence measurements in-vitro were acquired as mentioned in the in-vitro fluorescence measurement section. DEA-NONOate (Cayman) stock solution was added to a final concentration of 50 μM. Liquid H_2O_2 was used as H_2O_2 donor and its exact concentration was quantified using UV spectrophotometer ($\varepsilon = 43.6\ M^{-1}\ cm^{-1}$ at 240 nm). Xanthine/xanthine oxidase system was used for superoxide generation, which was quantified using Cytochrome C reduction as described[114]. Fenton chemistry reaction was used to generate hydroxyl radical ($^{\cdot}OH$)[115]. Aqueous solutions of NO_2^- and NO_3^- were prepared from their respective sodium salts. ROS and RNS generating small molecules were added to 100 nM of NOckout in 100 mM sodium phosphate buffer (pH 6.0), to a final concentration of 100 μM each of H_2O_2, $^{\cdot}OH$, $O_2^{\cdot-}$, NO_2^- and NO_3^-. 10 μM

NaOCl was added to generate 10 μM HOCl. Reaction mixtures were incubated at 37 °C for 15 min and fluorescence spectra were acquired in Alexa488 and DAR channels. Fold changes are reported in G/B and values were normalized to that of NOckout reacted with NO donor DEA-NONOate.

2.3 Results and Discussion

2.3.1. Determine pH sensitivity and specificity of NOckout probes

To study the NO-sensing properties of NOckout probes, we measured response kinetics of both NOckout probes upon addition of NO donor DEA-NONOate (50μM, pH6.0) by acquiring fluorescence emission spectra as function of time. DAR fluorescence increases rapidly, with ~80% of maximum signal response in <1 minute, while fluorescence intensities of normalizing fluorophores Alexa647 (R) and Alexa488 (B) remained constant over time. The NO response characteristics of both NOckout^{PM} and NOckout^{TGN} were pH insensitive in the range of 6-7.4. Both NOckout probes show maximum *in-vitro* fold change of ~6.5 (after to before addition of NO donor DEA-NONOate) viz. G/B for NOckout^{PM} and G/R for NOckout^{TGN} (Fig. 2.3).

Specificity of NOckout probes towards various ROS/RNS species and NO metabolites was checked by incubating NOckout^{PM} with 100 μM of generators of species of interest for 15 minutes at room temperature. 50 μM DEA-NONOate was used as a positive control (NO generator), DEA-NONOate showed ~6.5 fold change and since final concentration of NO donor was half that of other ROS/RNS, we can conclude that NOckout probes are at least 13-fold more selective to NO as compared to ROS/RNS analytes checked (Fig. 2.3f).

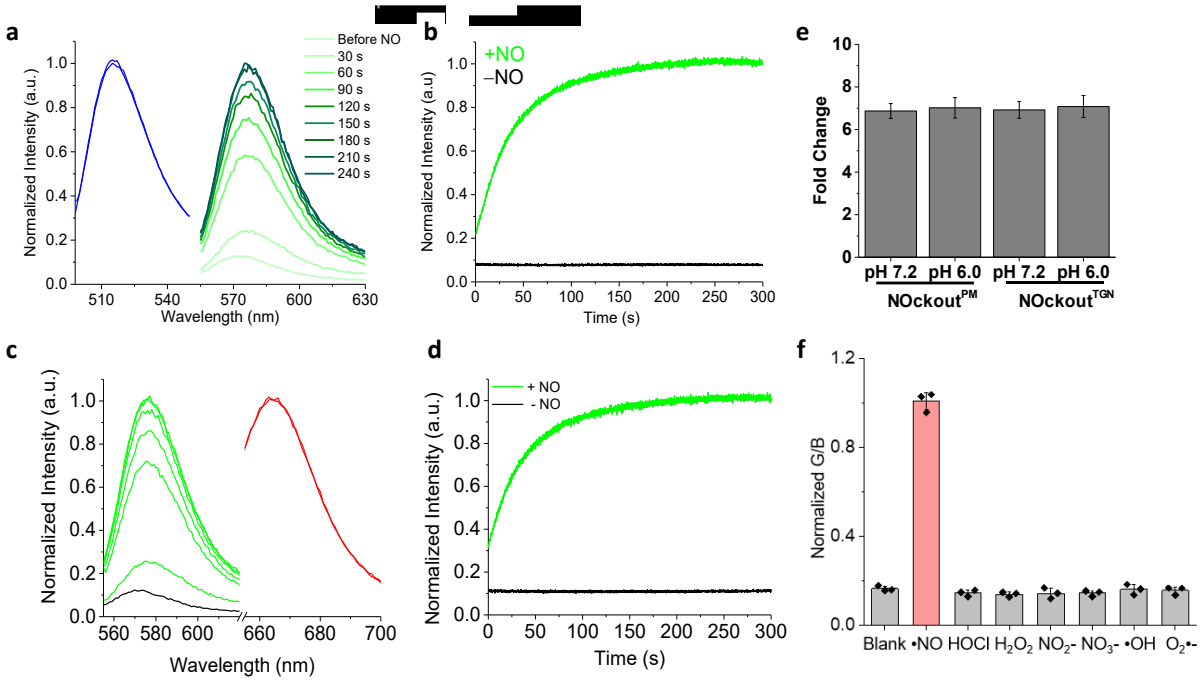

Fig. 2.3 Response characteristics of NOckout probes a. Fluorescence emission spectra of Alexa488 and DAR (NOckout^{PM}) obtained at indicated time points (30-second intervals for 3.5 minutes) after the addition of NO donor (DEA-NONOate, 50 µM, pH 6.0). DAR (λex= 554 nm) and Alexa488 (λex= 488 nm) are shown in color green and blue, respectively. **(b)** Representative kinetic trace of DAR in NOckout^{PM} (λex= 554 nm) upon addition of 50 µM DEA-NONOate, pH 6.0 (green) or DMSO (black). **(c)** Fluorescence emission spectra of Alexa488 and DAR (NOckout^{TGN}) obtained at indicated time points (30-second intervals for 3.5 minutes) after the addition of NO donor (DEA-NONOate, 50 µM, pH 6.0). DAR (λex= 554 nm) and Alexa647 (λex= 647 nm) are shown in color green and red, respectively. **(d)** Representative kinetic trace of DAR in NOckout^{TGN} (λex= 554 nm) upon addition of 50 µM DEA-NONOate, pH 6.0 (green) or DMSO (black). **(e)** Fold change (DAR intensity/reference fluorophore intensity) of NOckout variants upon treatment with DEA-NONOate in Phosphate buffer of pH 6.0 and pH 7.4, corresponding to the pH of the trans-Golgi lumen and extracellular space respectively. Error bars - S.E.M. from three independent experiments. **(f)** Sensitivity of NOckout^{PM} toward various reactive oxygen species or toward NO metabolites reported as normalized DAR/Alexa488 values. Error bars- standard error of mean from three independent experiments.

2.3.2 Targeting of NOckout probes

Despite evidence for NOS3 localization at the plasma membrane and the TGN, the relative activities of these distinct populations are still unknown[37,38,42,49]. Hence, we sought to map activities of NOS3 at these two locations by targeting spectrally distinct NOckout variants to either

location. 500 nM of NOckout^{PM} when incubated with T47-D, MCF-7 and diverse cancer cell types for 10 minutes showed robust labeling of plasma membrane, with CellMask^{TM} used as a plasma membrane marker in order to confirm targeting through colocalization (Fig. 2.4a). There was minimum or no internalization of NOckoutPM for the first 2 hours (Fig. 2.4c and Fig. 2.7). On the other hand, NOckout^{TGN}, was effectively endocytosed by a variety of epithelial cancer cell lines including T-47D cells, MCF-7, A549 etc. (Fig. 2.4d, d and Fig. 2.5). Colocalization with the TGN-marker BODIPY-C_5-ceramide confirmed that NOckout^{TGN} was localized to the TGN in these cell lines (Fig. 2.5). We also showed that NOckout^{TGN} doesn't localize to early endosomes, late endosomes or lysosomes by showing anti-colocalization with the endocytic tracer TMR-Dextran. TMR-Dextran, when pulsed continuously, labels all three aforementioned compartments (Fig. 2.6).

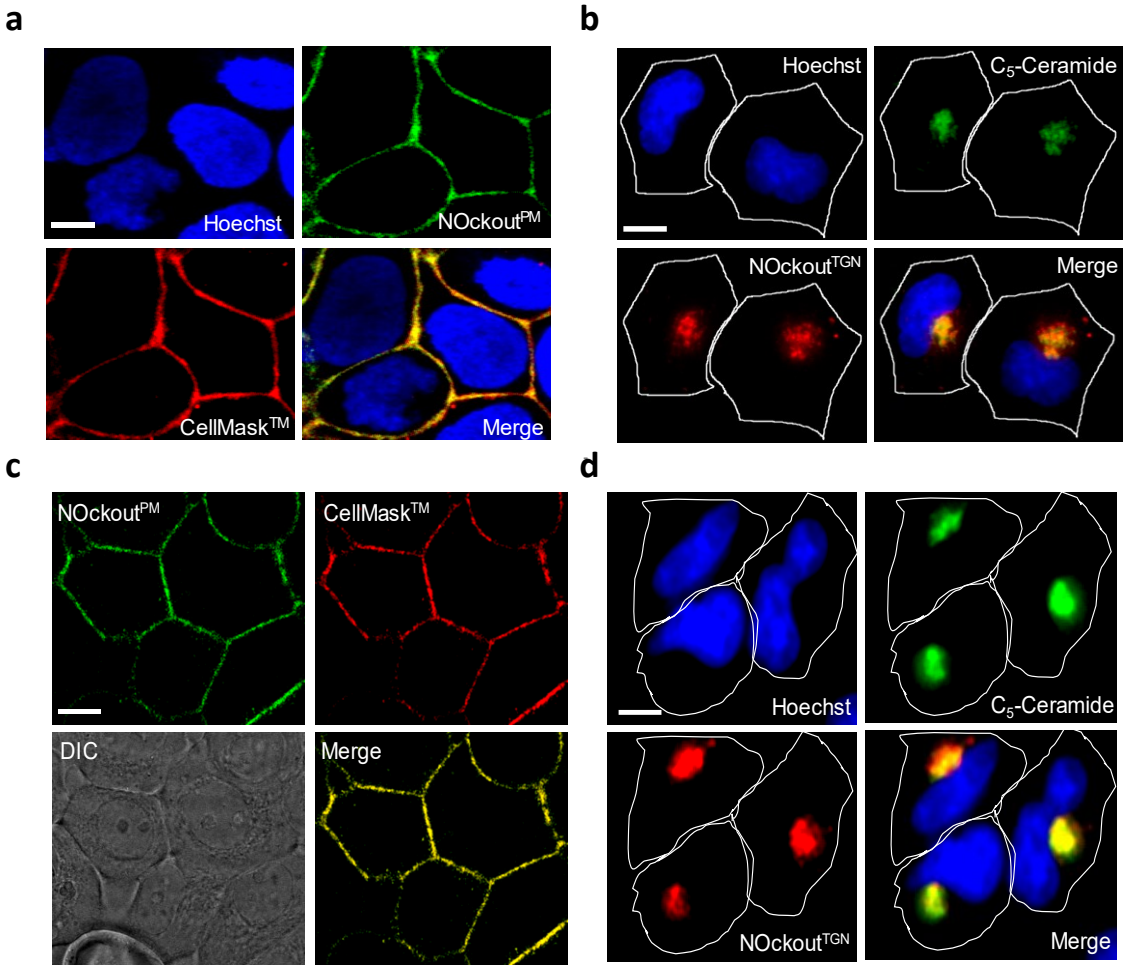

Fig. 2.4 Targeting of NOckout variants in T47-D and MCF-7 cells. (a) Confocal images show colocalization of NOckout^{PM} (λ_{ex} = 488 nm, green) with the plasma membrane stain CellMask^{TM} Red (red, λ_{ex} = 647 nm) in T-47D cells. **(b)** Confocal images show co-localization of NOckout^{TGN} (λ_{ex} = 647 nm, red) with trans-Golgi network stain C_5-Ceramide (λ_{ex} = 488 nm, green) in T-47D cells. **(c)** Confocal images show colocalization of NOckout^{PM} (λ_{ex} = 488 nm, green) with the plasma membrane stain CellMask^{TM} Red (red, λ_{ex} = 647 nm) in MCF-7 cells. **(d)** Confocal images show co-localization of NOckout^{TGN} (λ_{ex} = 647 nm, red) with trans-Golgi network stain C_5-Ceramide (λ_{ex} = 488 nm, green) in MCF-7 cells. Nuclei were stained using Hoechst 33342 (λ_{ex} = 405 nm, blue).. Scale bar: 10 μm.

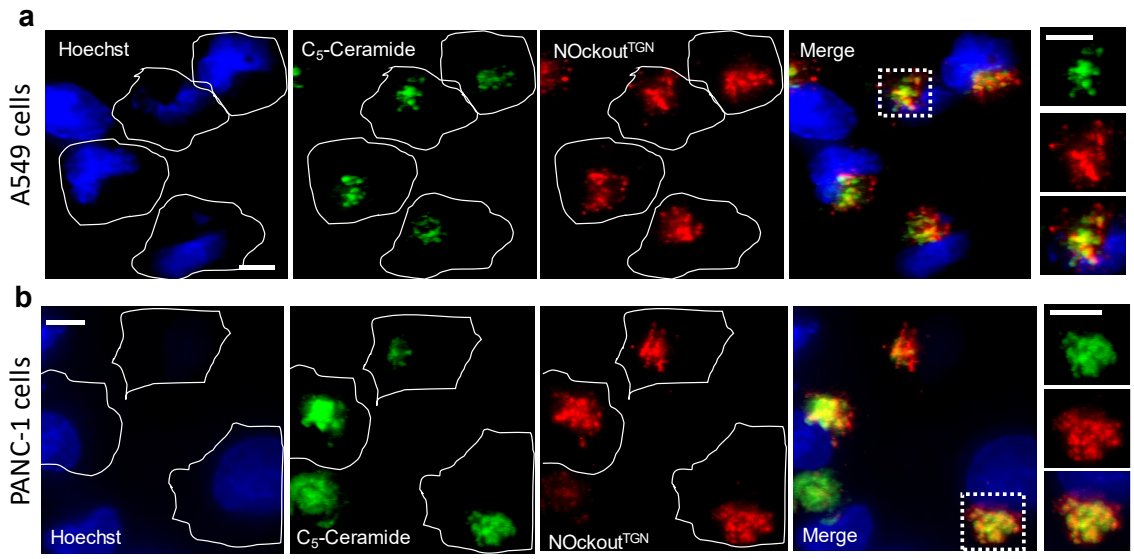

Fig. 2.5. NOckout^{TGN} localizes to TGN in lung and pancreatic carcinoma cells. Confocal images show co-localization of NOckout^{TGN} (red) with the trans-Golgi network stain C_5-Ceramide in **(a)** lung carcinoma cells A549 and **(b)** pancreatic tumor cells PANC-1. Hoechst 33342 is used as nuclear stain. Scale bar: 10 µm.

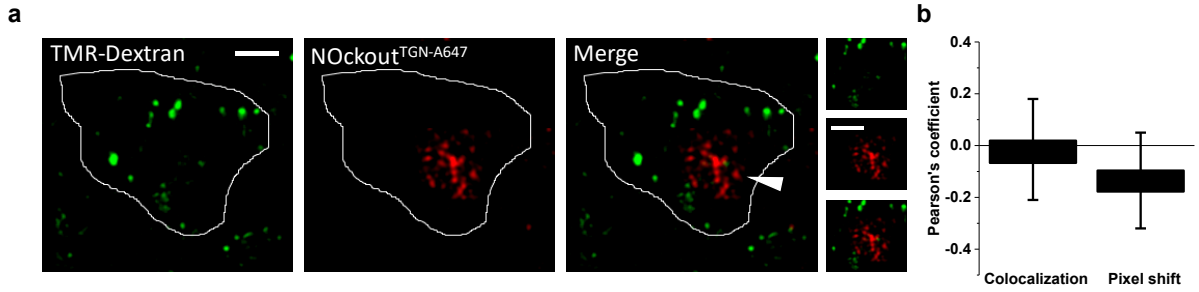

Figure 2.6. Anti-colocalization of NOckout^{TGN} with endocytic tracer TMR-Dextran. (a) Representative images showing cells where all endosomes are labeled with a continuous pulse of TMR-Dextran (green) and subsequently labeled with NOckout^{TGN} (red) **(b)** Pearson's correlation coefficient proves that NOckout^{TGN} does not localize to endosomes. n = 20 cells Error bars represent S.E.M. from two independent experiments. Scale bar: 10 µm.

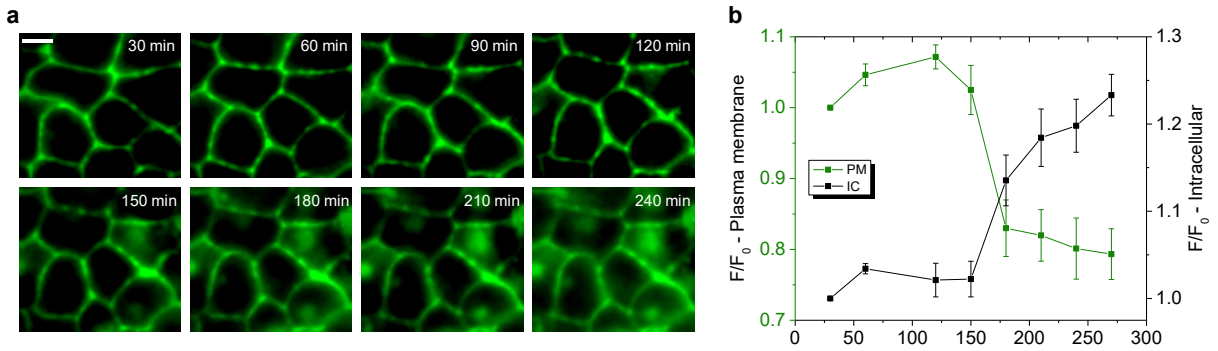

Figure 2.7. **Stability of NOckout^{PM} on the plasma membrane (a)** T-47D cells were incubated with 500nM NOckout^{PM} and were imaged every 30 minutes at room temperature in HBSS, Scale bar = 10 μm. **(b)** Quantification of NOckout^{PM} intensities for each time point at the plasma membrane as region of interest (PM) or intracellular space as region of interest (IC). Error bars represent S.E.M. from two independent experiments, n = 8 cells.

2.3.3 *In-cellulo* performance of NOckout probes

Next, we wanted to estimate endogenous NOS3 activity at the plasma membrane and Golgi without activating it by external means. First, we measured the ratiometric response of NOckout^{PM} (i.e. the G/B ratio), under conditions where NO was depleted inside cells using 300 mM NO scavenger 2-Phenyl-4,4,5,5-tetramethylimidazoline-1-oxyl 3-oxide (PTIO)[116]. We similarly measured the ratiometric response upon saturating the cell with NO using 500 mM DEA-NONOate, which completely turns on the NOckout probe and should yield the maximum G/B ratio. These two extreme scenarios provide the minimum and maximum G/B signals afforded by NOckout^{PM} in T-47D cells (Fig 2.8a-b). The G/B values under any subsequent treatments are normalized to that of the DEA-NONOate treated sample (maximum G/B signal). To measure basal NOS3 activity at the plasma membrane, we labeled cells with NOckout^{PM} and acquired steady state G/B values 1 h post-labeling (Fig 2.8a). Similarly, using ratiometric G/R values of

NOckout^{TGN} we obtained basal NOS3 activity at the TGN (Fig 2.8a-b). These results revealed that basal NOS3 activity was comparable at the plasma membrane and the Golgi (Fig 2.8b). When cells were treated with 1 mM L-N^{G}-Nitroarginine methyl ester (L-NAME), which inhibits all NOS isoforms, G/B and G/R values of NOckout probes gave similar values to those of PTIO-treated cells (Fig 2.8b)[117], whereas a NOS2 specific inhibitor, 1400W, had no effect (Fig 2.8b)[118]. This confirms that the ratiometric response of both the NOckout probes is due to the activity of NOS3 isoform and that the contribution of NOS2 is negligible in these cells under conditions used here (Fig 2.9 and Fig 2.10).

Next, we activated NOS3 using two different small molecule activators, both of which are associated with cancer etiology, and measured the steady state NOS3 activity at both sub-cellular locations. Addition of ATP activates Akt kinase via P_2Y_X receptors which phosphorylates NOS3 thereby increasing its efficiency to produce NO[48,119]. In contrast, 17β-Estradiol (E_2) increases cytoplasmic Ca^{2+} which activates NOS3 by increasing dwelling time of calmodulin (Fig 2.9)[120]. As expected, activating NOS3 by ATP addition gave significantly higher G/B and G/R ratios of NOckout^{PM} and NOckout^{TGN} respectively compared to basal levels (Fig 2.8b). To our surprise, E_2 selectively activated NOS3 only at the plasma membrane and Golgi NOS3 activity levels remained unchanged (Fig 2.8b).

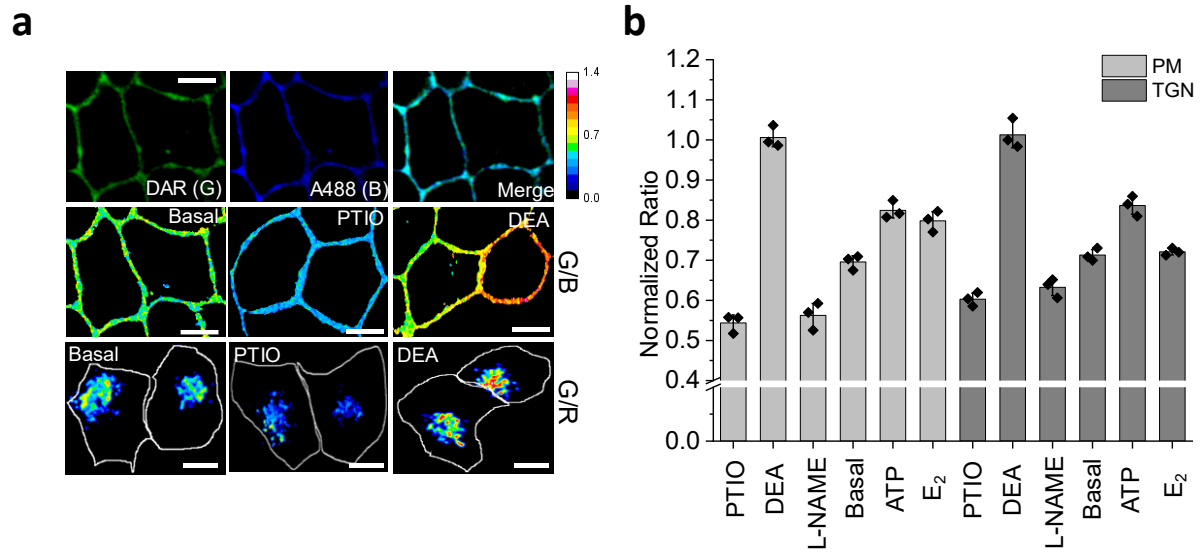

Fig. 2.8. NOckout devices map activities of NOS3 at the plasma membrane and at the Golgi **a**, NOckout^{PM} and NOckout^{TGN} maps endogenous NOS3 activity and modulations brought about by DEA-NONOate (300 µM, NO donor), PTIO (300 µM, NO scavenger) or in untreated cells (Basal) at the plasma membrane or at the Golgi of T-47D cells. DAR, A488 and A647 channels are shown in green (G), blue (B) and red (R) respectively, G/B and G/R ratios are shown in pseudo-color. Representative images are shown from a total of three independent experiments. **b**, Bar graphs showing the quantification of normalized G/B (NOckout^{PM}) or G/R (NOckout^{TGN}) ratios across six treatments (PTIO, DEA-NONOate, L-NAME, basal, ATP and E_2). PM, plasma membrane. Error bars represent standard error of mean from three independent experiments, $n \geq 35$.

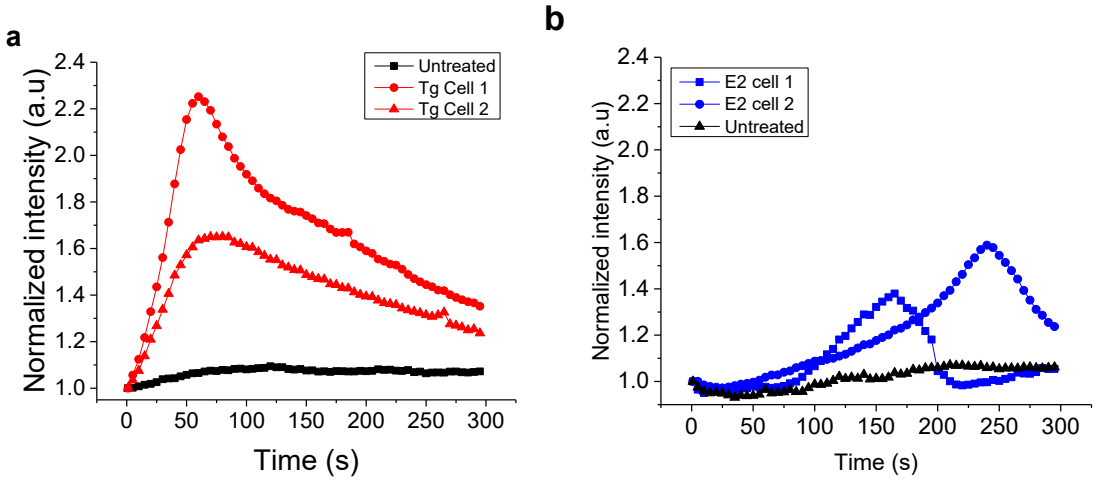

Figure 2.9: Intracellular calcium imaging followed by indicated treatments in T-47D. (a) Representative traces of cytosolic Ca^{2+} elevation from three different cells imaged with DAF-2

diacetate, a cytoplasmic calcium indicator (λ_{ex} = 488 nm). Cells were treated with 100 nM Thapsigargin (Tg, Red) or with vehicle (Black). **(b)** Representative traces of cytosolic Ca^{2+} elevation from three different cells upon treating cells either with 300 nM 17-β-Estradiol (E_2, Blue) or with vehicle (Black).

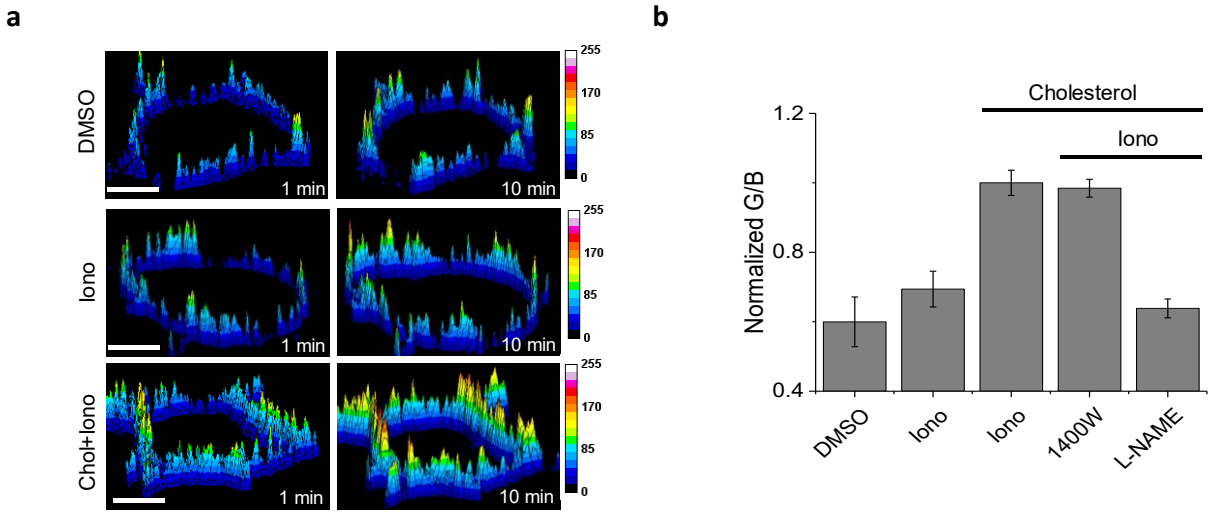

Figure 2.10: NOckout probes measure activity of NOS3 isoform and not that of NOS2. (a) Surface plots showing NOckout^{PM} labeled T-47D cells upon treatment with cholesterol + Ionomycin (Chol+Iono), Ionomycin (Iono) or DMSO (vehicle control). **(b)** Ratiometric response of NOckout^{PM} from T-47D cells acquired 10 min post treatment with DMSO, ionomycin (1 µM) or ionomycin in combination with cholesterol (500 µM) with or without 1400W or L-NAME. Error bars = standard error of mean, Scale bar = 10 µm and n = 20 cells.

2.3.4 Comparison with state-of-the-art NO probes.

We addressed benchmarking by a head-to-head comparison with two prime, commercially available, competitor probes: (i) a small molecule fluorophore, 4,5-Diaminofluorescein diacetate (DAF-2), used in 90% of all commercial cellular NO detection kits, and (ii) a recently developed genetically encodable protein-based sensor for NO called geNOp. NOckout outperforms both these excellent technologies on every parameter that we tested (Fig. 2.11 & 2.12 for results, Table 2 for summary), offering best of both worlds i.e., selective chemistry, photostability of small molecules and stable localization available to proteins.

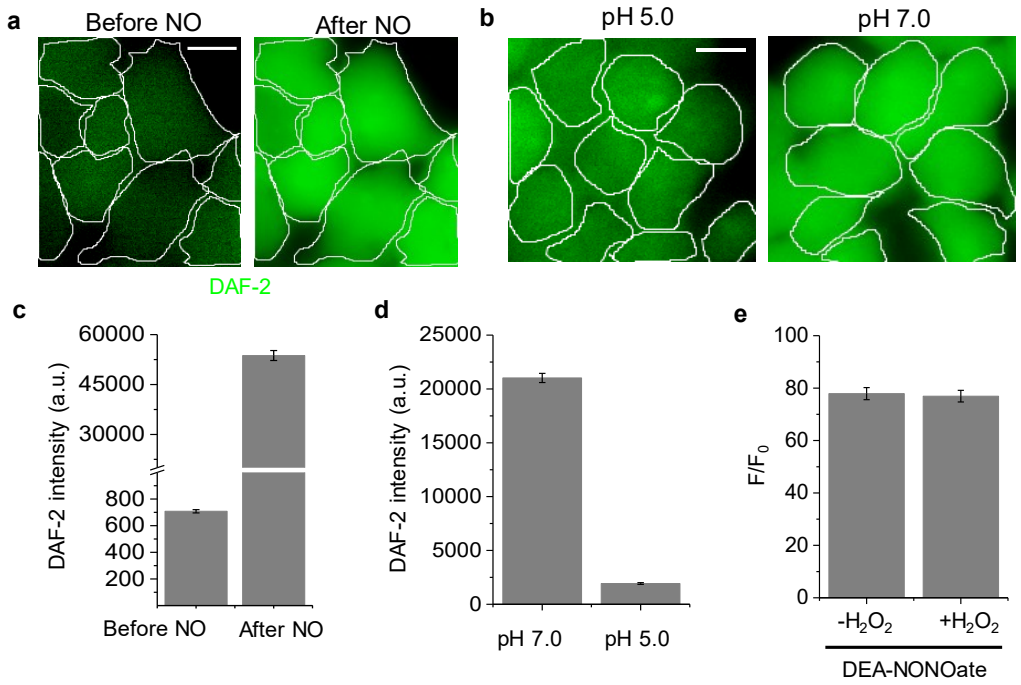

Figure 2.11: NO measurements using small molecule DAF-2DA. (a) Representative images of HEK cells loaded with DAF-2DA (10 μM) before addition of NO donor DEA-NONOate (Before NO) or 10 minutes after the addition of DEA-NONOate (500 μM, after NO), Scale bar = 10 μm. **(b)** Representative images showing HEK cells loaded with DAF-2DA and treated with DEA-NONOate were clamped at pH 5.0 or at pH 7.0. **(c)** and **(d)** are graphical representation where y-axis denotes whole cell DAF-2 intensities for experiments (a) and (b) respectively, where n=20 cells. **(e)** Bar graph showing fold changes in DAF-2 intensities of cells either pre-treated with H_2O_2 or pre-treated with H_2O ($-H_2O_2$) upon addition of DEA-NONOate (500 μM). Error bars are standard error of mean from three independent experiments.

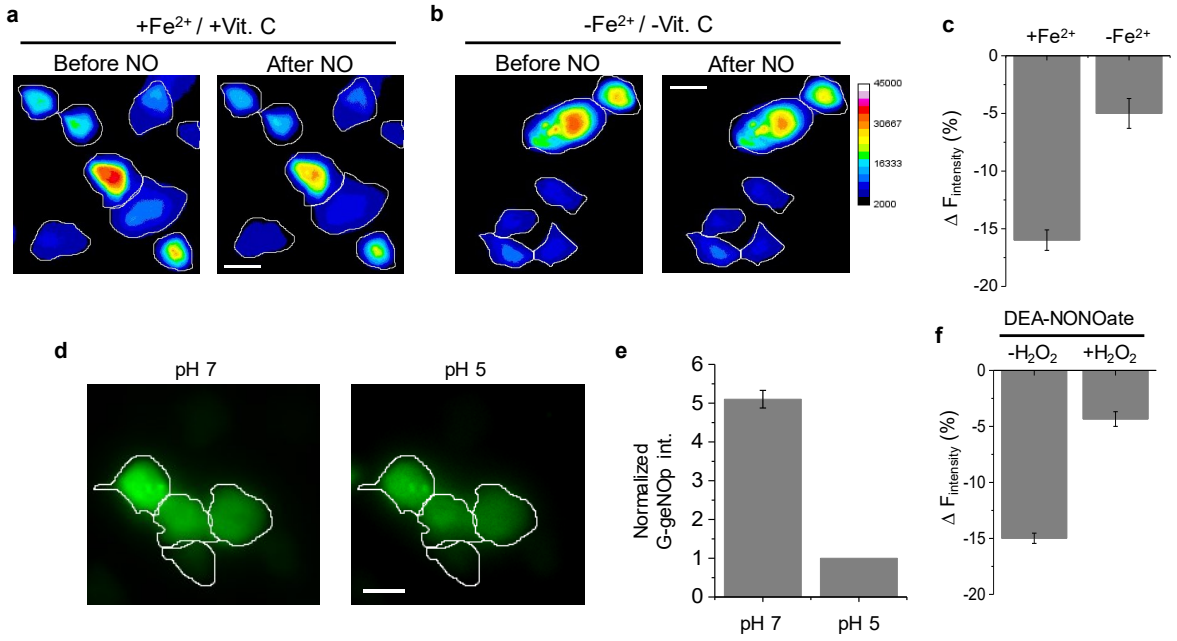

Figure 2.12: NO measurements using genetically encodable NO probe (G-geNOp). Representative pseudo-color images of HEK cells expressing cytoplasmic G-geNOp, where cells were treated with either Fe^{2+} and Vit. C **(a)** or in the absence of them **(b)**, before and after the addition of NO donor DEA-NONOate, Scale bar = 10 μm. **(c)** Bar graph showing delta fluorescence signal in percentage for (a) and (b), where n=20 cells. **(d)** HEK cells expressing cytoplasmic G-geNOp were pH clamped either at pH 5.0 or at pH 7.0 using UB4 buffer. **(e)** Whole cells G-geNOp intensities from (d), n=20 cells and Scale bar = 10 μm. **(f)** Bar graph showing delta fluorescence signal in percentage of cells expressing G-geNOp which were either pre-treated with H_2O_2 or pre-treated with H_2O ($-H_2O_2$) upon addition of DEA-NONOate (500 μM). Error bars are standard error of mean from three independent experiments.

Parameters	DAF-2DA[13] (commercial NO detection kits) (Fig S17)	G-geNOp[14] (protein sensor for NO) (Fig S18)	*NOckout* (this study)
Ratiometric	No (Fig. S17a)	No (Fig. S18a)	Yes (Fig. 1b-d and S1a-c)
Mode of sensing	Fluorescence turn on (Fig. S17a and c)	Fluorescence turn off (Fig. S18a and c)	Fluorescence turn on (Fig. S1b-c and S2a-b)
Sensitivity towards pH	Yes (Fig. S17b and d)	Yes (Fig. S18d-e)	No (Fig. S1d and S8e)
Cross-reactivity to H_2O_2	None (Fig. S17e)	Yes (Fig. S18f)	None (Fig. 1d)
Fe^{2+} supplementation	Not required (Fig. S17a and c)	Required (Fig. S18a-c)	Not required (Fig. S1b-c and S2a-b)
Maximum in-cellulo fold change	7500% (Fig. S17c)	-15% (Fig. S18c)	200% (Fig. 1f)
Organelle targetability	No (Fig. S17a)	Yes[14]	Yes (Fig. S2c-d, S3 and S4)
Reversible	No[13]	Quasi-reversible[14]	No (Fig. S1b-c and S2a-b)

Table 2: Benchmarking NOckout against commercially available NO probes (adapted from Jani et al., *Nature Chemical Biology* (2020)[1].

2.4 Response to "News and Views"

A News and Views article titled "Yes (again) to local NO" on this work was published online on 22nd May in *Nature Chemical Biology*[121]. First of all, I congratulate the authors for capturing the essence of our findings, enlisting its potential uses and discussions of a broader outlook. However, there were couple of instances where statements were either inaccurate or misleading to the readers. I would like to address these incorrect statements in this thesis,

a. **"Diaminorhodamine (DAR) fluorophore derivative that irreversibly reacts with the NO radical to form a bright green fluorescent triazole"** – The fluorescence emission maxima of DAR triazole is 572 nm, whereas green fluorophores have emission wavelengths in the range of 500-520 nm. By not emitting in green wavelengths, NOckout

probes avoid autofluorescence associated with green spectrum and are compatible with probes/markers which uses GFP/FITC based cores.

b. **"Although other intracellular membranes also contain cholesterol, so the specificity of the targeting is not absolute" ….. "because the authors have not reported the subcellular distribution of the 'untargeted' NOckout construct, the precise role of the cholesterol moiety in targeting remains undefined"** – Cholesterol-conjugated oligonucleotides have been targeted to the plasma membrane and experimentally characterized in terms of biological impact by You *et al.*[108]. We and others have utilized this strategy in more than 10 different types of cell lines for targeting oligonucleotides to the plasma membrane[102,108,122,123].

c. **"MUC1 undergoes dynamic targeting to multiple intracellular organelles, of which the Golgi network is but one of many"** – The authors cite an article which deals with tracking of C-terminal domain of MUC1 which is generated after the full length MUC1 is cleaved. The full-length protein is known to shuttle between the Golgi apparatus and plasma membrane[124,125]. We used an aptamer which binds to the hypo-glycosylated N-terminal of MUC-1. In this case, the aptamer conjugated to NOckout^{TGN} should be ferried it to the Golgi apparatus by full-length MUC-1 (Fig. 2.13). This aptamer was described first by Ferreira et al., and has been shown to target Golgi apparatus in certain epithelial cancer cell lines[110]. We also showed anti-colocalization of NOckout^{TGN} with vesicular compartments using the pan-endosomal marker TMR-Dextran (Fig. 2.6) again showing specificity of NOckout^{TGN} targeting.

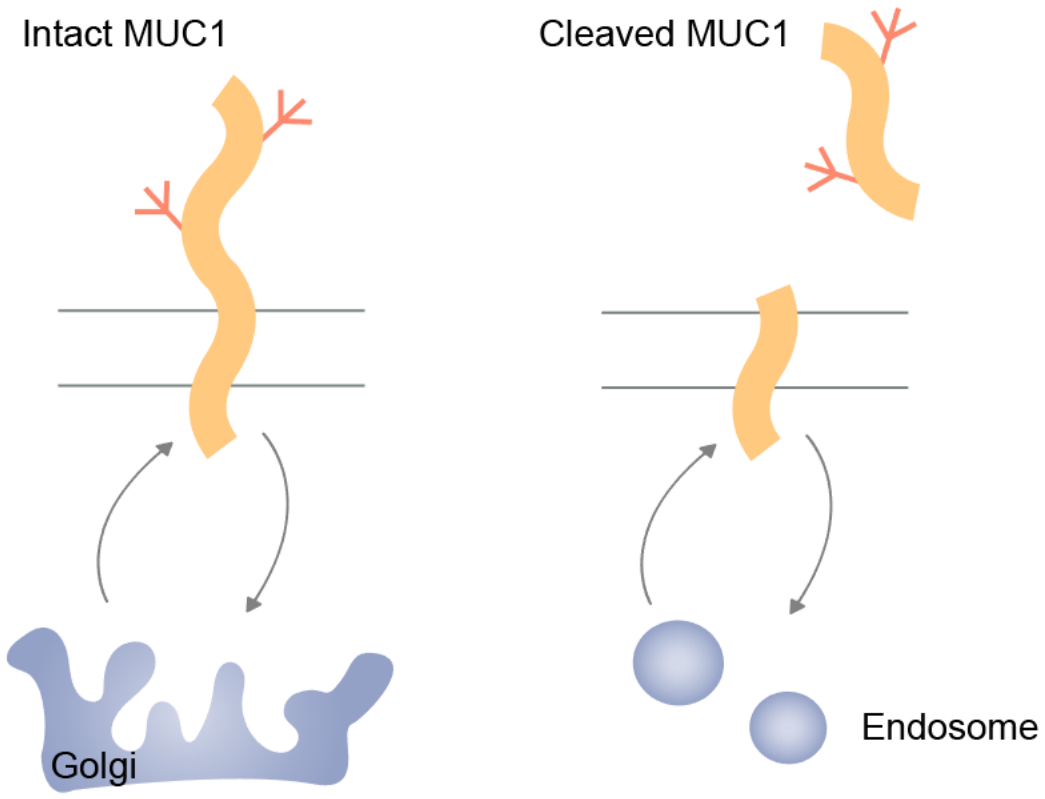

Fig. 2.13. Schematic depicting trafficking routes taken by MUC1. Intact hypo glycosylated MUC1 shuttles between the trans-Golgi network and the plasma membrane whereas, C-terminal of cleaved MUC1 traffics to the endo-lysosomal compartments.

d. **"However, a recent study attested to a clear discordancy in phosphorylation-dependent NOS3 activation"** – The authors mention a finding that reveals that phosphorylation of NOS3 alone is not an effective proxy of NOS3 activity and whenever NOS3 phosphorylation is used as proxy for NOS3 activity, it should be supported with NO and Ca^{2+} imaging inside cells[126]. The way it is articulated implies that it is applicable for our study. We use NOckout to monitor NOS3 activity by NO production, which is true measure of NOS3 activity. We treated cells with an agonist that increase intracellular Calcium showed NOS3 phosphorylation and increase in NO production. Given this, there

is no discordancy between NOS3 phosphorylation and NOS3 activation in the system we have published on.

It is important to be as clear and accurate as possible when discussing a novel finding so as not to misguide readers. We believe we have clarified some of these statements to better articulate the true potential of NOckout probes with this reply.

2.5 Conclusion

We designed NOckout probes using DNA as scaffolding material. We showed that NOckout probes outperform current state-of-the-art small molecule and genetically encodable probes. NOckout probes are highly selectivity towards NO and show 14-fold selectivity when compared with other ROS and NO metabolites which the probe might encounter within the cell. NOckout probes can be targeted to the Golgi apparatus and plasma membrane of a number of epithelial cancer cell lines. To show generality we used breast, pancreatic and lung carcinoma cells in this chapter. Favorable maximum percentage signal change of 200% in-cellulo allows one to detect small changes in NO levels. The fast response times and pH-insensitivity of these probes position them well to map NOS3 activities at the plasma membrane (pH 7.4) and the TGN (pH ~6.0)[93,127].

Chapter 3

Quantitative subcellular imaging of NOS3 activity

3.1 Introduction: Sub-cellular NOS3 populations and their roles

Nitric Oxide modifies ~1000 proteins and regulates their activity to eventually regulating multiple signaling pathways[128–130]. Therefore, NOS activity is tightly controlled transcriptionally and and post-translationally. For example, NOS3 is regulated by a variety of post-translational modifications, such as phosphorylation, sub-cellular sequestration and protein-protein interactions[3,43,48]. Phosphorylation of NOS3 at Serine-1177 increases its activity presumably by increasing calcium sensitivity and/or by increasing reductase activity[3,42]. In endothelial cells, NOS3 localizes to cholesterol-rich domains of the plasma membrane and to the *trans*-Golgi network[119,131]. Localization of NOS3 to these distinct sub-cellular organelles is achieved by post-translational modifications such as myristoylation and palmitoylation at the N-terminal domain of NOS3[3,8,37,40]. Myristoylation mediates targeting of NOS3 to the Golgi-Apparatus and palmitoylation of two different cysteine residues enables NOS3 translocation to the plasma membrane. Mutations at the myristoylation site lead to mis-localization of NOS3. It remains in cytoplasm and shows reduced enzyme activity[37,39]. Sub-cellular populations of NOS3 are posited to play specific physiological functions. For example, the Golgi-associated NOS3 population is known to promote tumor maintenance and tumor growth whereas NO released from cells due to the activity of plasma membrane-associated NOS3 is believed to play a role in cardio-vascular diseases[119,132,133]. The abundance of NOS3 at each location and the activity of each population are predicted to vary between cell types and across different species. Moreover, the amount of NO that each population produces in each case is not known. Developing technologies to measure

relative activities of sub-cellular NOS3 populations would help us better understand the role of these populations in physiology and pathophysiology.

Zhang et al., generated an endothelial cell line and attempted to study the relative activities of NOS3 populations[119,133]. In these cells they knocked down endogenous NOS3 and transfected either the NOS3 variant that localizes selectively to the plasma membrane via a CAAX motif or transfected with the NOS3 variant that localizes to the Golgi-apparatus using an S17 targeting sequence[119]. Since these cells express only one specific sub-cellular population of NOS3, the total amount of NO produced upon various pharmacological perturbations can be ascribed to a single population. Using this approach, the authors demonstrated that plasma membrane localized NOS3 was more efficient (~7 fold more NO production) in NO production compared to the Golgi-localized population[119]. Since *NOckout* probes can be selectively targeted to the plasma membrane and the Golgi, we sought to develop a method to simultaneously measure NO produced by endogenous NOS3 populations in real-time with sub-cellular resolution. We used NO-production rate provided by the respective probes to compute the sub-cellular NOS3 activity at single cell resolution.

3.2 Materials and Methods

Immunofluorescence staining

T-47D and MCF-7 were cultured on a glass bottom (10 mm diameter) 3.5 cm imaging dish until they reach 60% confluency. Cells were treated with small molecule NO scavengers (20 μM methylene blue, 20 μM hemoglobin and 100 μM PTIO), iNOS inhibitor (10 μM 1400W) or small molecule ROS scavenger (2 mM TEMPOL). After the treatment, cells were washed three times with 1× PBS (pH 7.4) and were fixed by paraformaldehyde, final concentration 4% for 15 minutes at room temperature. Subsequently, cells were permeabilized using triton X-100 (final concentration 0.25%) followed by blocking using BSA (3% final concentration in 1× PBS). Cells were the incubated with monoclonal or polyclonal primary antibodies: mouse monoclonal anti-eNOS antibody (SantaCruz Cat# sc-376751), Rabbit Polyclonal anti-*S*-nitrosocysteine antibody (Abcam Cat# ab94930 or Abcam Cat# ab50185), Rabbit polyclonal anti-Giantin antibody (Abcam Cat# ab24586) or Mouse monoclonal Anti-GM130 antibody (BD Biosci. Cat# 610822). These antibodies were diluted in blocking buffer (3% BSA in 1× PBS) and incubated with cells for 1 hour at room temperature. Cells were subsequently washed with 1× PBS (3 times, 5 min each wash). Cells were incubated with respective secondary antibodies conjugated with either Alexa488 or Alexa647 (diluted in blocking buffer) for 1 h at room temperature. Cells were washed with 1× PBS for 5 min each (3×) to remove excess secondary antibody. 5 μM Hoechst 33342 was added to stain nuclear DNA for 10 min just before imaging. Images of stained cells were acquired using Leica SP8 laser scanning confocal microscope using excitation wavelengths of 405 nm for Hoechst, 488 nm for Alexa488 and 647 nm for Alexa647. Images were processed using Fiji/Image J and maximum *z* stack projection of 2–3 *z*-planes were used in representative images.

Sub-cellular nitric oxide quantification

Quantification of NOS3 activity was performed as described in Jani et al., (2020)[1]. We consider only the first 30 seconds of the rate curve in our analysis. During *in-cellulo* experiments, we took images every minute and hence we take the slope of the first minute after the DEA-NONOate addition as the initial rate of G/B increase, because Fig. 3.3d shows that the slope of the first minute whether images are taken at 1 frame/10 s or at 1 frame/1 min remains the same. For every $[NONOate]_0$, we plot the initial rate of d[NO]/dt from predicted [NO] curve against initial rate of G/B from *in-cellulo* experiments, which gave a linear curve with linear fit (R^2=0.97) and confirms the approximation assumed in equation 3. We use this calibration curve for the measurements of rate of NO produced by NOS3 populations.

Using this calibration curve, we plugged in the initial rates of G/B increase from thapsigargin treated T-47D cells and measured the rate of plasma membrane NO production to be 576±61 nM/s (Fig. 3.2c). Next, in order to measure NO production at the Golgi and to directly use calibration curves that we generated for the plasma membrane, we did two important control experiments. First, we proved that the DAR reaction kinetics to form DAR-T is independent of the pH of solution. Since NOckout^{PM} and NOckout^{TGN} sees pH units of 7.4 and 6 respectively (pH of PM and Golgi respectively), we checked reaction kinetics of DAR by utilizing pH insensitive NO donor S-Nitroso-N-acetyl-DL-penicillamine (SNAP, 1 mM)[138](Fig. 3.3e). We found that DAR has the same reaction kinetics at both pH 6.0 and pH 7.4 Second, we confirmed that the photo-physical properties of the normalizing dye (Alexa647 for NOckout^{PM} and Alexa488 for NOckout^{TGN}) do not alter ratiometric responses of NOckout probes. To achieve this, we designed NOckout^{PM} with either Alexa488 as the normalizing fluorophore or Alexa647 as the normalizing fluorophore and

measured their ratiometric response on the plasma membrane as a function of time upon treatment with 500 mM of DEA NONOate in T-47D cells. We found that the response kinetics of G/B or G/R increase of NOckout$^{PM-A488}$ or NOckout$^{PM-A647}$ is the same and doe not change upon changing the normalizing fluorophore (Fig. 3.3f). After ruling out these two parameters, we plugged in the initial rate from Golgi NOS3 activity (NOckout^{TGN} containing T-47D cells treated with 1 mM thapsigargin) and found the rate of NO production to be 74±41 nM/s.

3.3 Results and Discussion

3.3.1 Time-lapse imaging of NOS3 activity at the Golgi and plasma membrane

We showed in chapter 2 that the NOckout probes could report NOS3 activity at steady state with sub-cellular resolution. Next, we sought to map NOS3 activity in real-time. Cytosolic Ca^{2+} elevation is known to activate both plasma membrane and Golgi NOS3 populations in the cell[41]. Although, Zhang et al. suggested that NOS3 at the plasma membrane is more active, this is based on available extracellular NO_2^- and NO_3^-, which are by-products of the resultant NO produced[41,119]. In order for NO metabolites to be available for measurement in the extracellular space, NO produced at the Golgi has to cross through a ~5 mM barrier of cytoplasmic thiols without being scavenged. Therefore, the relative activity of NOS3 pools remains unknown and can only be resolved by measuring activities directly at the site of production.

To measure NO production rates from sub-cellular NOS3 pools, we labeled the plasma membrane and the Golgi of T-47D with *NOckout^{PM}* and *NOckout^{TGN}* simultaneously. Co-localization with Golgi and plasma membrane markers confirmed that both the NOckout probes can be targeted

simultaneously in same cells (Fig. 3.1a). To map activities of NOS3 populations at both sites simultaneously, we treated these dually labeled cells with 1 μM thapsigargin. Thapsigargin increases cytoplasmic [Ca^{2+}] by blocking Sarco/endoplasmic reticulum Ca^{2+}-ATPase (SERCA). Preventing Ca^{2+} reuptake by the ER activates calmodulin, which then binds to NOS3 and activates it[139]. Fluorescence images of stimulated, dually labeled cells were acquired in the Alexa488 (B), DAR (G) and Alexa647 (R) channels as a function of time (Fig. 3.1b). The G/B ratio at the plasma membrane followed a sigmoidal increase as a function of time, while at the TGN, G/R ratio started to increase slowly only after 3 minutes (Fig. 3.2a). G/B and G/R values of the cells treated with PTIO stayed fairly constant over the experimental timescales, indicating that fluorophore bleaching and non-specific probe reactivity in cells were negligible (Fig. 3.2a).

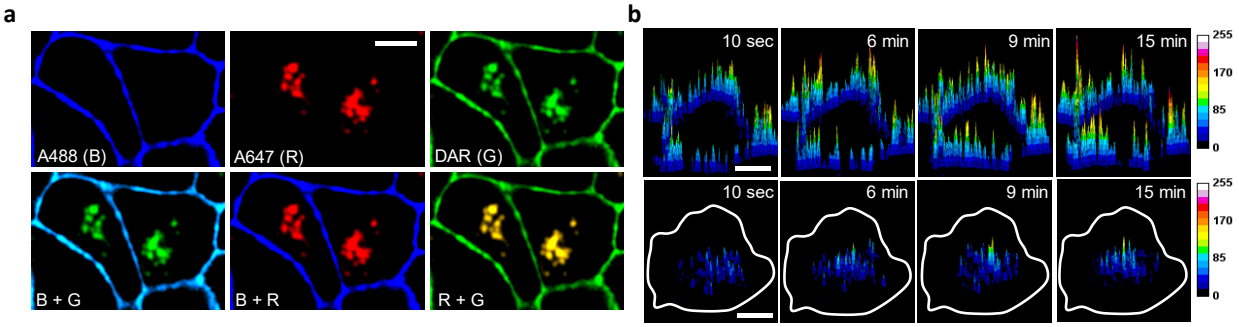

Fig. 3.1 Simultaneous, quantitative NO mapping from two distinct subcellular locations (a) Simultaneous incubation of 500 nM NOckout^{PM} and 500 nM NOckout^{TGN} on T-47D cells results in labeling of both plasma membrane and Golgi of the same cell. **(b)** *NOckout^{PM}* and *NOckout^{TGN}* maps live NO production upon stimulation with 1 μM thapsigargin. Single plane images were acquired every 3 min for 24 min on a confocal microscope. NO ratiometric responses are calculated as DAR/A488 (in the case of *NOckout^{PM}*) and DAR/A647 (in the case of *NOckout^{TGN}*) and are represented as surface plots.

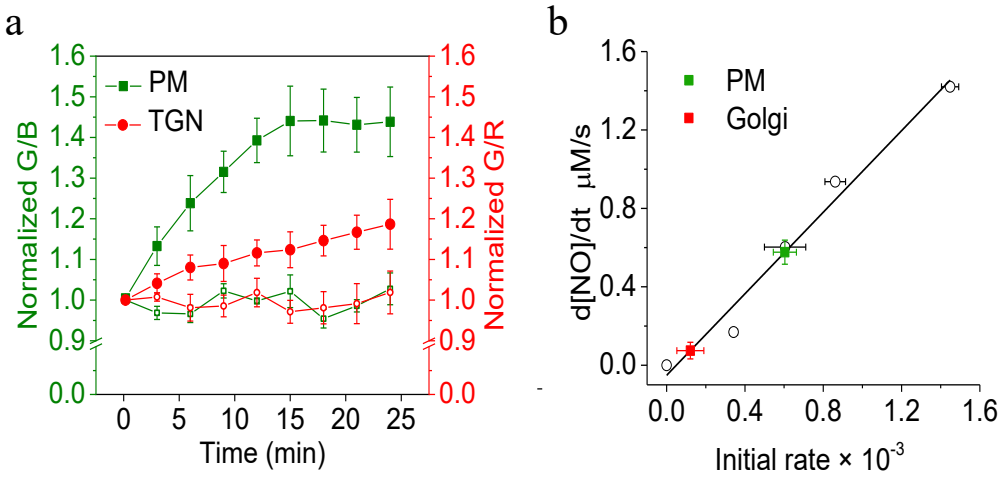

Figure 3.2. **Mapping of NOS3 enzymatic activity simultaneously at two sub-cellular locations. (a)** Kinetic traces of NOS3 activity from the plasma membrane (green) and the Golgi (red) in live T-47D cells. Simultaneous signal increase from *NOckout*^{PM} and *NOckout*^{TGN} are recorded as a function of time from single cells treated eiher with thapsigargin (filled squares and circles) or with PTIO (empty squares and circles). Mean intensities are plotted as ratios of DAR/Alexa488 (G/B, *NOckout*^{PM}) and DAR/Alexa647 (G/R, *NOckout*^{TGN}) for total of 10 cells, error bars - standard error of mean. **(b)** *In-vitro* (d[NO]/dt) vs. *in-cellulo* (initial rate × 10^{-3}) plot overlaid with initial rates for 1 µM Tg treated cells (green filled square - plasma membrane and red filled square, Golgi) calculated from Fig. 3.2a . error bars - standard error of mean.

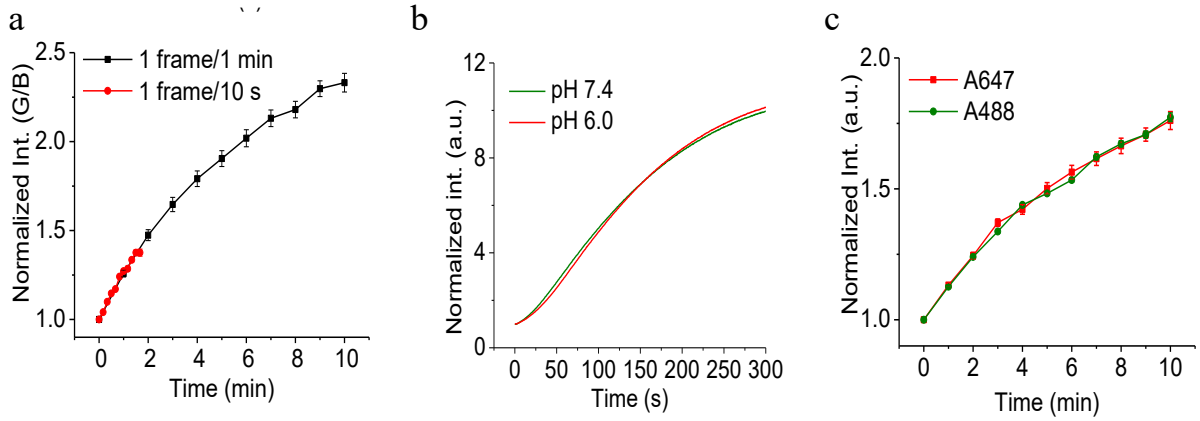

Fig. 3.3: Quantification of enzymatic activity using NOckout probes. (a) NOckout^{PM} labeled cells were treated with 500 mM of DEA-NONOate and their ratiometric responses were recorded either at 1 frame/1 min (black trace) or at 1 frame/10 s (red trace). **(b)** *in-vitro* DAR reaction kinetics upon incubation with of 500 µM of SNAP either at pH 6.0 (200 mM phosphate buffer, red trace) or at pH 7.4 (200 mM phosphate buffer, green trace). **(c)** Reaction kinetics comparison of T-47D cells labeled with NOckout^{PM} containing either Alexa647 as ratiometric fluorophore (red

curve) or Alexa488 as ratiometric fluorophore (green curve) upon addition of 500 μM of DEA-NONOate.

3.3.2 Quantification of NOS3 activity at the Golgi and plasma membrane.

Next, in order to measure the relative activities of NOS3 sub-populations, we developed a method to quantify NO generated at both locations. The concentration of NO, a reactive species, changes with time; it increases due to enzymatic activity and reaches a maximum value[134]. When this activity stops, NO levels decrease because of diffusion, dismutation or reaction with other molecules (Fig. 3.3a-b)[140]. As the effective concentration of NO ($[NO]_{eff}$), changes with time, accurate NOS3 activity is best quantified by the rate of NO production. Therefore, we first measured the decomposition rate constant (k_1 sec^{-1}) of DEA-NONOate by monitoring UV absorbance at 250 nm, to obtain $[NO]_{eff}$ over time in solutions containing range of DEA-NONOate concentrations (Methods section)[136]. From these $[NO]_{eff}$ vs time curves, we obtained the initial rates of NO production (Fig. 3.3b).

Next, we developed an in-cell calibration protocol to measure the rate of NO production using NOckout^{PM} devices for range of DEA-NONOate concentrations. We added a fixed concentration of DEA-NONOate to cells labeled with NOckout^{PM} and recorded ratiometric response (G/B) as a function of time. The mean G/B value from ~20 cells yielded sigmoidal curves as a function of time (Fig. 3.2a). Utilizing this we could calculate initial rates of ratiometric increase of NOckout^{PM} for each DEA-NONOate concentration. These *in-cellulo* rates were plotted against its corresponding *in-vitro* rate of NO production (Fig. 3.2b-c). This gives us a linear calibration curve which helps to determine ratiometric responses of NOckout^{PM} for different initial rates of NO production. Next we treated NOckout^{PM} labeled cells with 1 μM thapsigargin and measured the rate of NO production by ratiometric response. Extrapolation of this rate on the NOckout^{PM}

calibration curve gives us an NO production rate of 576±61 nM/sec by NOS3 at the plasma membrane (Fig. 3.2c).

NOckout^{TGN} localizes in the lumen of the Golgi apparatus, which has a pH of ~6.2[127]. However, reaction kinetics of DAR with NO is pH-insensitive and as expected, the response characteristics of NOckout probes at pH 6.0 and 7.4 are identical (Fig. 3.3e-f). Due to these similarities, we could directly compare the rate of NO production of *NOckout^{TGN}* labeled cells treated with 1 μM thapsigargin with the in-cell calibration curve. Calculating this gave us an NO production initial rate of 74±41 nM/sec for the Golgi associated NOS3 population. Interestingly, the rate of NO production at the plasma membrane was ~7 times greater than that of Golgi (Fig. 3.2c). Next, we investigated whether these differences in activities arose due to the relative abundances of NOS3 at the plasma membrane and the Golgi. Counterintuitively, immunostaining for NOS3 revealed that major fraction corresponding to ~60% was localized at the Golgi, whereas only ~40% of total cellular NOS3 was localized at the plasma membrane (Fig. 3.4). Taking this factor int consideration, NOS3 at the plasma membrane is actually ~10 fold more active than at the Golgi.

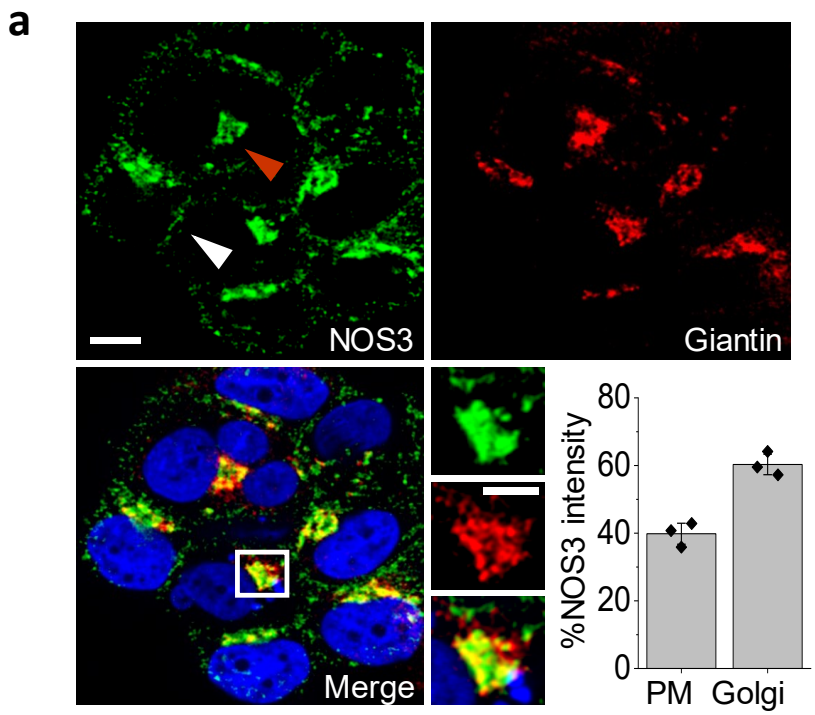

Figure 3.4. Relative NOS3 abundance at plasma membrane and the Golgi. (a) NOS3 (green) co-localization with the Golgi apparatus marker protein Giantin (red) in T-47D cells. Higher magnification images are shown in the inset. NOS3 population at the plasma membrane and at the Golgi are represented with white and maroon arrowhead respectively. Bar graphs show percentage of NOS3 located at the PM and at the Golgi. Error bars - standard error of mean, n = 50 cells, Scale bar = 10μm.

3.3.3 Phosphorylation of NOS3 S1177 increases PM associated NOS3 activity.

Next, we attempted to understand the mechanism behind this difference in the activities of NOS3 populations. Phosphorylation of Serine 1177 (S1177) on NOS3 by Akt kinase is known to make it more efficient at producing NO, probably by stabilizing the NOS3-calmodulin complex and/or by recruiting Hsp90[43,48]. However, direct evidence of population specific phosphorylation of Serine-1177 in cells has not yet been observed. To investigate whether differences in phosphorylation levels might account for the activity difference between populations, we immunostained NOS3 with two different antibodies. One of the antibodies selectively binds S1177

phosphorylated NOS3 (P-NOS3) and the other binds all NOS3 molecules irrespective of its phosphorylation status (Fig. 3.5). Normalized ratio of P-NOS3/total NOS3 shows that plasma membrane NOS3 population is ~7 times more phosphorylated at S1177 than the Golgi population (Fig. 3.5). This favored phosphorylation of S1177 NOS3 at the plasma membrane could explain its higher activity. This result is in agreement with biochemical studies on synthetic NOS3 variants that suggest NOS3 at the plasma membrane is preferentially phosphorylated[119].

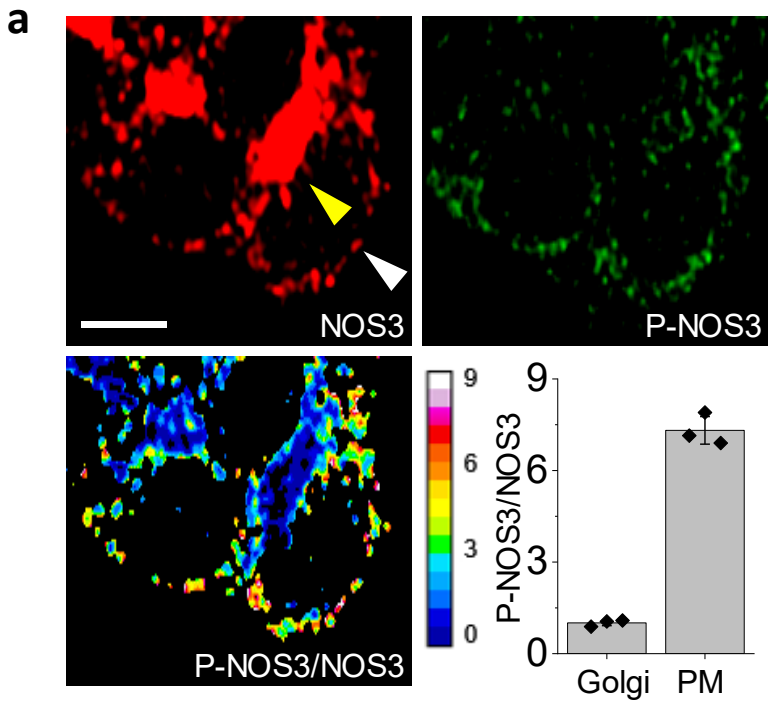

Fig. 3.5. Plasma membrane NOS3 population is preferentially phosphorylated. (a) Immunostaining of NOS3 and S1177 phosphorylated NOS3 (P-NOS3) in T-47D cells. Heatmap of P-NOS-3/NOS3 image shows the extent of phosphorylation. White arrowheads represent plasma membrane associated NOS3 population and yellow arrowheads represent Golgi associated NOS3 population. Bar graphs show quantification of the same. Error bars - standard error of mean, n = 30 cells, Scale bar = 10µm.

3.4 Conclusion

By quantitatively mapping activities of both sub-cellular NOS3 pools in the same cell using NOckout probes, we found that plasma membrane associated NOS3 selectively gets activated upon

cytoplasmic Ca^{2+} elevation. These results are in agreement with studies in endothelial cells expressing either plasma membrane targeted or Golgi-apparatus targeted synthetic NOS3 variants[38,119]. We directly compared activities of endogenous NOS3 pools in single cells using NOckout and found that NOS3 was 10-fold more active at the plasma membrane as compared to that at the TGN, suggesting that the NOS3 populations might be differentially regulated. Indeed, the plasma membrane associated NOS3 is phosphorylated at position Ser1177 whereas Golgi population lacks such a modification.

Chapter 4 The Golgi is a hotspot for S-nitrosylation

4.1 Introduction: Protein S-nitrosylation and its biological functions

NO regulates numerous important signaling pathways in all life forms[14,141,142]. It was recognized early on that one of the ways in which NO regulates functions of various proteins is by direct attachment of NO to the heme moiety in proteins such as guanylate cyclase[143]. Covalent modification of cysteine residues by NO (S-nitrosylation) to form the S-NO bond leads to a post-translational modification called S-nitrosylation. The chemical species which leads to S-nitrosylation of Cysteine thiols might involve NO_x, an autooxidation product of enzymatically produced NO[128,144,145]. S-NO modification is known to control protein activity by changing proximal electrostatic charges, hydrophobicity, orientation of aromatic side chains, distance between targeted cysteine and transition metal or redox center, or by changing protein-protein interactions. Further, S-NO modification can inhibit or facilitate di-sulfide bond formation in a protein[128]. Approximately one thousand proteins in mammalian cells are estimated to undergo S-nitrosylation[146]. A substantial amount of prior work have shown the direct effect of S-nitrosylated endogenous proteins in numerous signaling pathways in physiology and in pathophysiology[147–149].

Although most known cell types contain one or more NOS isoforms and almost all known proteins have at least one Cysteine residue, endogenous S-nitrosylation is highly substrate specific. Moreover, in almost all the proteins which are regulated by S-nitrosyation, only one or few of the Cys residues are modified[150]. A few of the factors which might play a role in determining this specificity are electrostatic interactions that modify pKa and hence the nucleophilicity of thiol

residues, accessibility of thiol groups, interaction of NOS isoforms with target proteins or proteins which can transfer NO groups, etc[128].

S-nitrosylation controls protein players involved in cell growth, apoptosis and angiogenesis[151,152]. Recent research has demonstrated that S-nitrosylation is one of the key factors which affects every phase of cancer cell progression[130]. Some well-known onco-proteins which can be regulated by S-nitrosylation are listed below in Table 3. For example, c-Src is a tyrosine kinase, known to facilitate cancer cell invasion and metastasis. Interestingly, NO stimulation increases the activity of c-Src. Mass-spec based analysis showed that c-Src can be S-nitrosylated at position Cys498 by NO which stimulates its kinase activity[153]. This cysteine is conserved among other members of human Src family kinases such as, c-Yes and c-Fyn[153,154].

Protein	***SNO site***	***Effect***
RAS[132,155]	158, 229	Anti-apoptotic
Bcl-2[156]		
P53[157]	Unknown	Anti-apoptotic
MKP-1[158]	258	Anti-apoptotic
Fas[159]	199, 304	Pro-apoptotic
Hif-1a[160]	533	Pro-angiogenesis
Dynamin[161]	86, 607	Pro-angiogenesis
MKP-7[162]	244	Pro-angiogenesis
PTEN[163]	Unknown	Pro-angiogenesis
c-Src kinase[153]	498	Pro-invasion and metastasis
O6-alkylguanine transferase[164]	145	Pro-development

Table 3: List of onco-proteins known to get regulated by S-nitrosylation.

Protein S-nitrosylation is strictly regulated both spatially and temporally[165–167]. Temporal control is achieved by accessory factors that facilitate or inhibit S-nitrosylation/de-nitrosylation, and the

spatial control is achieved by subcellular localization of NOS isoforms[128,165]. The cellular redox environment also plays a role in S-nitrosylation by sequestering NO as GS-NO[168].

Analysis of the dissociation energies required to cleave the S-N bond in S-NO has shown that homolytic decomposition of this bond is not feasible under physiological conditions[169,170]. Hence, de-nitrosylation in cells should happen either by transfer of the NO group or through reductive mechanisms. De-nitrosylation in cells has been shown to be carried out either by enzymes such as superoxide dismutase (SOD) and by oxidoreductase like thioredoxin (TRX)[171,172]. Both these proteins have been shown to reverse S-nitrosylation *in-vitro* (from small molecules) and TRX has been shown to de-nitrosylate *in-vivo*[128].

In this chapter, I describe the contribution of sub-cellular NOS3 pools in S-nitrosylation of proteins. I have also studied the roles of S-nitrosylated proteins in the regulation of Golgi morphology and cell growth in human breast cancer cells. We have also used pharmacological screening to investigate the player(s) and mechanisms involved in the regulation of NO mediated signaling in the Golgi Apparatus.

4.2 Results and discussion

4.2.1 Golgi is an S-nitrosylation station

In cancers, plasma membrane-associated population of NOS3 might be able to mediate processes such as angiogenesis and metastasis through regulating trans-membrane proteins such as E-cadherin, EGFR and matrix metalloproteinases[173]. Golgi associated NOS3 in our case has 1/10th of NO production rate as compared to plasma membrane population. To dissect the role of the hypoactive Golgi associated population NOS3 (discussed in chapter 3, section 3.2), we used an

anti-S-nitrosocysteine antibody to detect S-NO levels in T-47D and in MCF-7 cells. Co-immunostaining with bona fide Golgi-resident protein GM130 showed significant colocalization between S-nitrosocysteine staining and the Golgi marker in both T-47D cells and MCF-7 cells (Fig. 4.1 and Fig. 4.2). However, MCF-10A and 184A1, breast epithelial cell lines isolated from normal individuals, showed no anti-S-nitrosylation immunostaining at the Golgi apparatus (Fig. 4.3). In T47-D cells, immunostaining data showed significantly higher intensity of anti-S-nitrosylation staining at the Golgi apparatus as compared to plasma membrane. This observation was surprising as the steady state level of basal NOS3 activity at the plasma membrane and the Golgi are comparable in our experiments. Treatment of cells with NO scavenger PTIO showed significant decrease in S-nitrosylation intensity at the Golgi (Fig. 4.4), whereas treating cells with a NOS2 specific inhibitor, 1400W, led to no change in S-nitrosylation intensity at the Golgi apparatus, confirming that NOS3 is the isoform responsible for protein S-nitrosylation at the Golgi apparatus (Fig. 4.5).

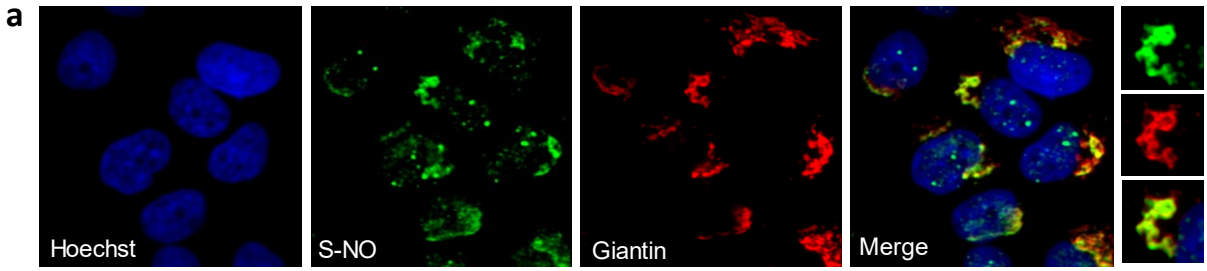

Fig. 4.1 Golgi acts as a S-nitrosylation hotspot in breast cancer cells. (**a**) Extensive endogenous *S*-nitrosylation of Golgi proteins in T-47D cells (green), shown by colocalization with Golgi marker protein GM-130 (red). Higher magnification images are shown in the inset. Representative confocal stacks are shown from a total of three independent experiments.

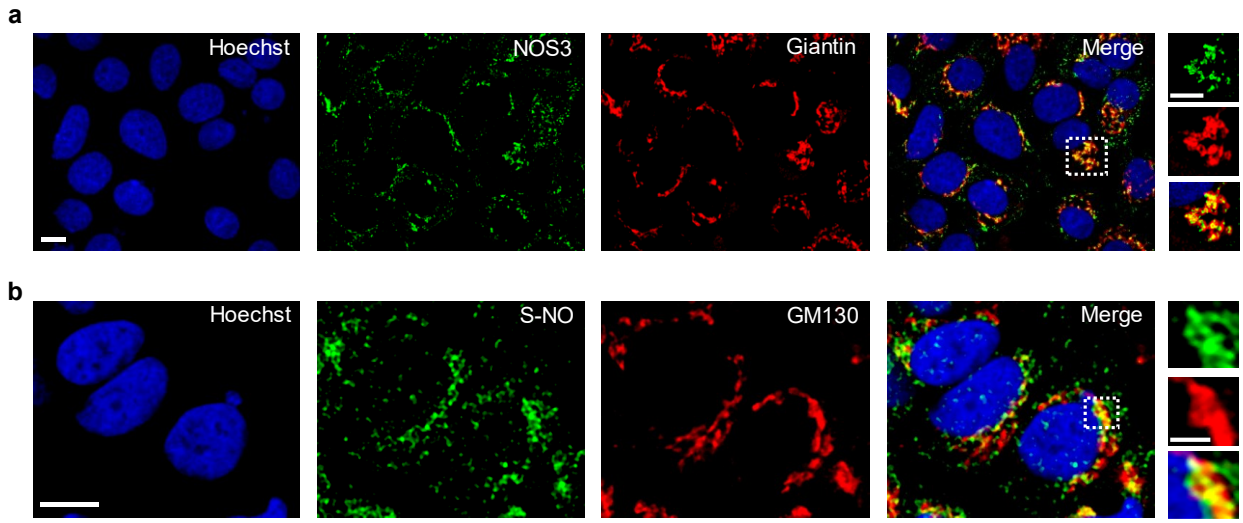

Figure 4.2: Golgi is a hotspot for S-nitrosylation in MCF-7 cells. (a) Confocal images show co-localization of NOS3 protein (green) with the Golgi resident protein Giantin (red) in MCF-7 cells. **(b)** Confocal images show co-localization of S-nitrosylated proteins (green) with Golgi marker protein GM-130 (red). Insets shows images in higher magnification. Scale bar: 10 μm. Interestingly, prolonged incubation of cells with L-NAME, a pan NOS inhibitor significantly reduced protein S-nitrosylation at the Golgi.

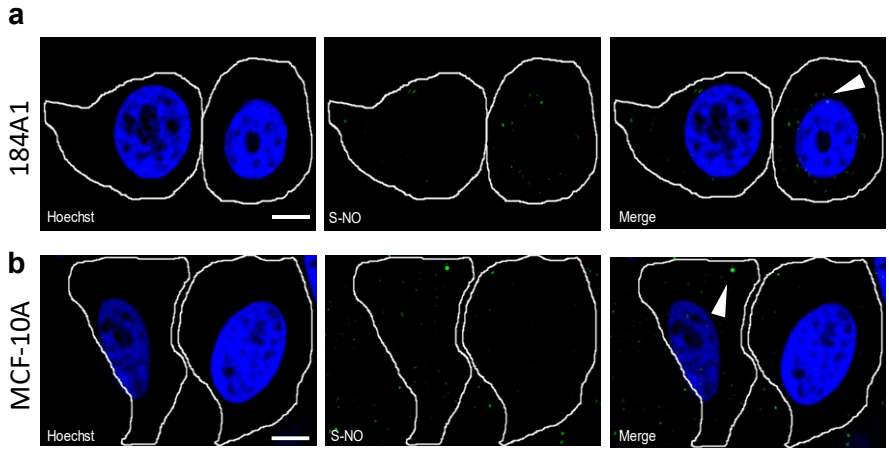

Fig. 4.3: S-nitrosylation in breast epithelial cell lines derived from normal individual. Immunostaining of S-nitrosylated proteins (green) in normal human breast cell lines **(a)** 184A1 and **(b)** MCF-10A. Hoechst (blue) was used to stain nuclei. Scale bar = 10 μm.

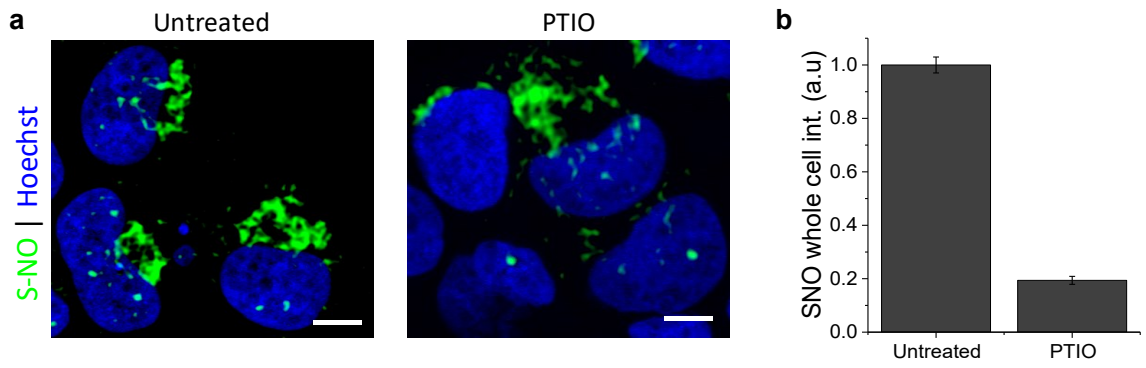

Fig. 4.4: PTIO mediated NO scavenging reduces extent of S-nitrosylation. (a) Representative images showing immune-stained S-nitrosylated proteins in T-47D cells treated with or without 200 mM PTIO for 48 hours. **(b)** Quantification of whole cell anti-S-nitrosylation intensity. n = 150 cells, Scale bar: 10 μm. Error bars – standard error of mean from three independent experiments.

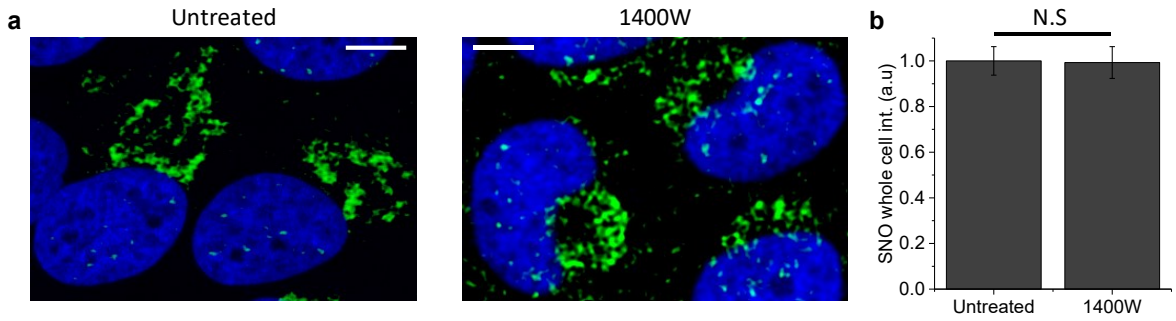

Figure 4.5: NOS2 isoform does not play role in S-nitrosylation of Golgi proteins. (a) T-47D incubated with or without 10 mM of iNOS inhibitor 1400W for 48 hours followed by immunostained with anti-S-nitrosocysteine antibody (green). **(b)** Quantification of whole cell anti-S-nitrosylation intensity. n = 200 cells. Significance as given by two tailed students T test. N.S = non-significant, Scale bar: 10 μm and Error bars – standard error of mean from three independent experiments.

4.2.2 S-nitrosylation of Golgi proteins is required for its structural integrity

Prolonged L-NAME treatment in our experiments leads to Golgi fragmentation as shown by anti-GM130 immunostaining (Fig. 4.6 and Fig. 4.10). This fragmented Golgi morphology was also observed when the T-47D cells were treated with small molecule NO specific scavengers like PTIO, Methylene Blue (MB) and Hemoglobin (HB) (Fig. 4.6). Similar results were observed in

MCF-7 cells upon treatment with NO scavengers (Fig. 4.7). These results show that the Golgi apparatus is an S-nitrosylation hotspot, and this protein S-nitrosylation is essential for the maintenance of Golgi architecture in breast cancer cells. Furthermore, along with Golgi fragmentation, small molecule mediated NO scavenging also resulted in cell senescence and impeded cell growth (Fig. 4.8 and Fig. 4.9). This is in agreement with other studies where S-nitrosylation of Golgi-associated onco-proteins such as H-Ras, N-Ras and GOLPH3 are associated with tumorigenesis and cancer progression[132,174].

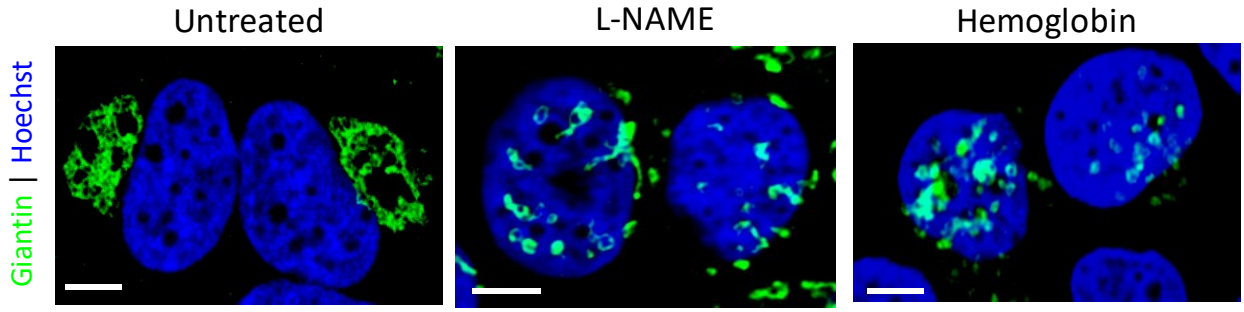

Figure 4.6: NO scavenger treatment causes Golgi fragmentation in T-47D cells. Immunostaining using anti-Giantin antibody (green) of untreated cells or cells treated with Methylene blue (20 mM) or Hemoglobin (20 mM). Hoechst (Blue) is used to stain nuclei. Scale bar: 10 μm.

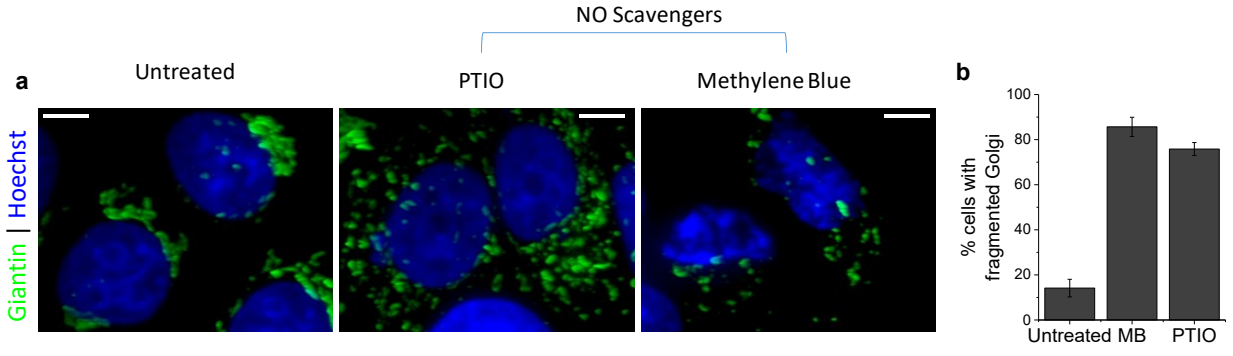

Figure 4.7: NO scavenger treatment causes Golgi fragmentation in MCF-7 cells. **(a)** Immunostaining using anti-Giantin antibody (green) of untreated cells or cells treated with Methylene blue (20 mM) or PTIO (100 mM). Hoechst (Blue) is used to stain nuclei. Scale bar: 10

μm. **(b)** Quantification of fragmentation. Error bars represent standard error of mean from three independent experiment; n = 150 cells.

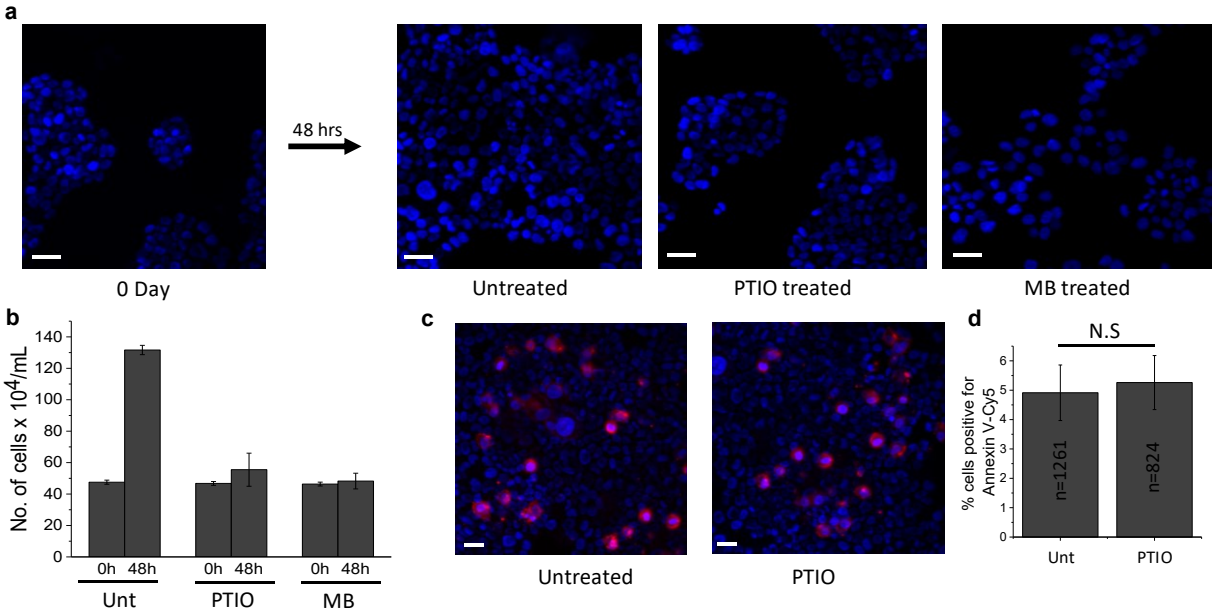

Figure 4.8: NO Scavenging hampers growth rate of T-47D cells. (a) T-47D treated with PTIO (200 mM), Methylene blue (MB, 20 mM) or DMSO (nbtreated) for 48 hours. **(b)** Number of cells were quantified after 48 hours of PTIO or MB treatment compared to DMSO treatment (untreated). **(c)** DMSO treated T-47D cells or PTIO treated cells were stained with apoptotic cell marker Annexin V-Cy5 (Biovision 1013-200). **(d)** Quantification of cells in **(c)**. Error bars represent standard error of mean from three independent experiment; n = 50 cells. Significance from two tailed students T test. N.S = non-significant. Scale bar = 50 μm. Hoechst (blue, λ_{ex} = 405 nm) was used as nuclear stain.

To test whether the cell growth retardation caused by NO scavenging was due to apoptosis, we stained cells treated with PTIO with a fluorescent apoptotic marker, Annexin V-Cy5 (Fig. 4.8). Results showed that NO depletion did not cause significant differences in cell apoptosis. However, when we tested for β-galactosidase activity as a proxy for cell senescence it revealed that PTIO treated cells showed a two-fold increase in cell senescence as compared to DMSO treated cells (Fig. 4.9)[175].

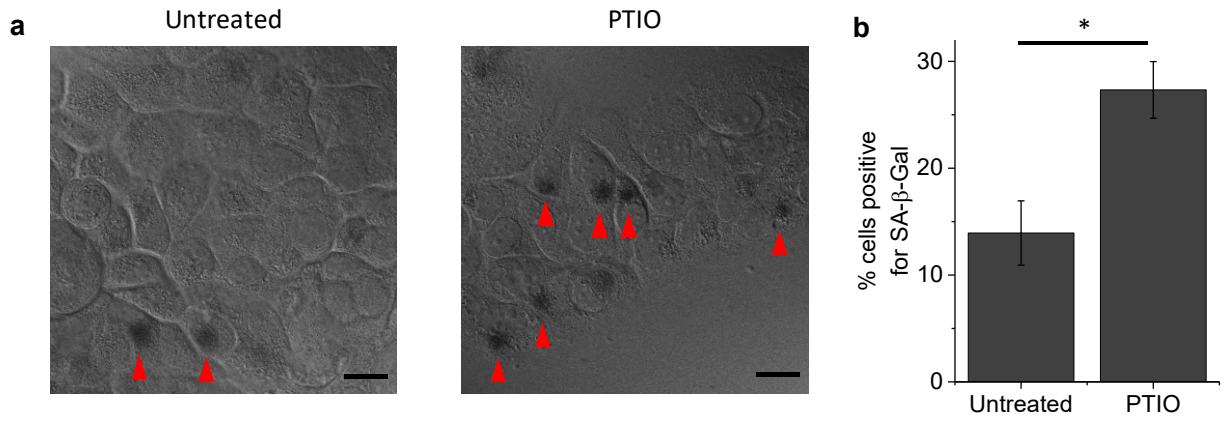

Figure 4.9: NO scavenging results in cell-senescence. (a) Cells incubated with or without PTIO (200 mM), stained for b-galactosidase (SA-b-Gal) activity. **(b)** Bar graphs showing percentage of cells positive for SA-b-Gal activity for the indicated treatment. Error bars show standard error of mean from three independent experiments and n = 200 cells. Significance as given by two tailed students T test. *$p < 0.05$, Scale bar = 10 μm.

4.2.3 Src kinases are responsible for NO scavenging mediated Golgi fragmentation

Next, to identify molecular players responsible for NO scavenging-mediated Golgi fragmentation, we performed a pharmacological screening using small molecule inhibitors. Rationale behind the screen is that inhibiting the function of a protein responsible for methylene blue-induced Golgi fragmentation should block this fragmentation. To rule out any contribution from reactive oxygen species (ROS)-producing enzymes or from NOS2 isoforms, we used ROS specific small molecule scavenger, 4-Hydroxy-2,2,6,6-tetramethylpiperidinyloxy (TEMPOL) and NOS2 specific inhibitor 1400W[176], and neither of these molecules fragmented the Golgi apparatus(Fig. 4.10). We treated cells with small molecule cGMP phosphodiester inhibitor, sildenafil citrate, an immediate downstream molecular player involved in NO signaling cascade. This treatment did not fragment the Golgi apparatus, ruling out the role of NO-induced activation of cGMP synthase in Golgi fragmentation (Fig. 4.10b). Initiation of apoptosis activates Rho A kinase, which leads to Golgi fragmentation[176]. Treating cells with the Rho A kinase specific small molecule inhibitor Y-27632

did not prevent MB-induced Golgi fragmentation, ruling out roles of Rho A kinase and apoptosis in this process (Fig. 4.10b). Next, we used a range of small molecule inhibitors against kinases that have been known to play roles in Golgi fragmentation under various physiological and pathophysiological conditions. We inhibited DNA-PK that is known to fragment Golgi by phosphorylating GOLPH3 upon DNA damage[174]. Treating cells with NU7441, a DNA-PK specific small molecule inhibitor did not prevent MB induced Golgi fragmentation, ruling out DNA-PK's role in this process[174]. Inhibitors containing an indirubin core are known to inhibit a number of Cyclin dependent kinases (CDKs) and Src family kinases[177]. We treated cells with two indirubin core containing inhibitors, indirubin-e804 (I-E804) and indirubin-3'-monoxime (I-3'M). Both these compounds completely prevented MB-induced Golgi apparatus fragmentation (Fig. 4.10b). (R)-Roscovitine is a broad inhibitor of CDKs and using (R)-Roscovitine (Rosco), we ruled out roles of CDK1, CDK2 and CDK5 in MB induced Golgi fragmentation. Interestingly, SU6656, an Src kinase inhibitor, which inhibits at least four members of human Src family kinases, reduced NO depletion mediated Golgi fragmentation by ~50%[178]. Treating cells with actin polymerization inhibitor Latrunculin B (LatB) completely blocked Golgi fragmentation, revealing the role of actin polymerization in MB-induced Golgi fragmentation (Fig. 4.10b)[179]. These results led us to propose a model to explain NO scavenging mediated Golgi fragmentation (Fig. 4.10c).

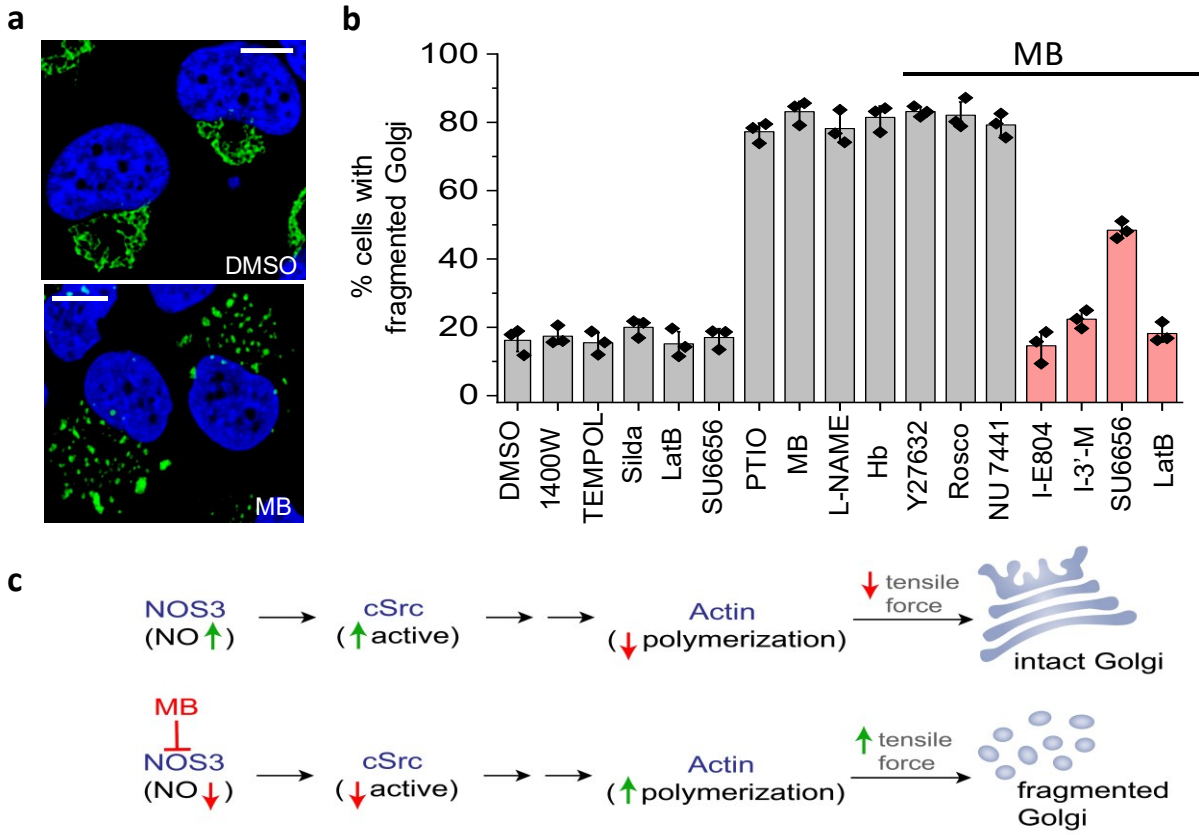

Figure 4.10. **Src family kinases regulates NO scavenging mediated Golgi fragmentation (a)** Treating cells with small molecule NO scavenger methylene blue (MB) results in Golgi fragmentation. Fragmented Golgi is visualized through Giantin immunostaining (green) as a highly vesicular structure DMSO treatment was used as negative control and did not result in Golgi fragmentation. **(b)** Small molecule inhibitor screen results were quantified as the percentage of cells with fragmented Golgi upon indicated small molecule treatment. Hoechst (blue) was used to stain nuclei, Scale bar = 10µm, error bars represent standard error of mean, n = 200 cells. **(c)** Proposed model depicts players involved in NO scavenging mediated Golgi fragmentation. S-nitrosylation of cSrc by NOS3 increases its activity. This active cSrc is known to reduce actin polymerzation, which results in decreased pull force and an intact Golgi. On the other hand, when NOS3 is inhibited or NO is scavenged, cSrc activity decreases due to less S-nitrosylation, which leads to increased actin polymerization, increased pull force and hence Golgi fragmentation.

4.3 Conclusion

Despite the low activity of Golgi associated NOS3 population, we detected extensive *S*-nitrosylation at the Golgi apparatus in breast cancer cells. This suggests that slow yet sustained NO production from Golgi associated hypo-active NOS3 population is responsible for S-

nitrosylation of Golgi proteins. This *S*-nitrosylation of Golgi associated proteins is absolutely required for the maintenance of Golgi morphology. Golgi apparatus integrity is maintained by NOS3 via cSrc kinase and an Actin-mediated mechanism, which when disrupted leads to cell senescence and growth retardation. HRas, NRas and GOLPH3 are Golgi associated proteins and S-nitrosylation of these is known to regulate cancer progression[71,132,174]. In fact, undergoing senescence by Golgi fragmentation promotes cell survival by inhibiting apoptosis[174]. We think that depleting protein S-nitrosylation of Golgi associated proteins in breast cancer cells might act as a fail-safe mechanism, where the cell could avoid undergoing apoptosis until environmental conditions become favorable for growth.

4.4 Data availability

The data that support the plots within this paper and other findings of this study are available from the corresponding author upon reasonable request.

References

1. Schuman, E. M. & Madison, D. V. A requirement for the intercellular messenger nitric oxide in long-term potentiation. *Science* **254,** 1503–1506 (1991).

2. Rapoport, R. M., Draznin, M. B. & Murad, F. Endothelium-dependent relaxation in rat aorta may be mediated through cyclic GMP-dependent protein phosphorylation. *Nature* **306,** 174–176 (1983).

3. Förstermann, U. & Sessa, W. C. Nitric oxide synthases: regulation and function. *Eur. Heart J.* **33,** 829–37, 837a (2012).

4. MacMicking, J., Xie, Q. W. & Nathan, C. Nitric oxide and macrophage function. *Annu. Rev. Immunol.* **15,** 323–350 (1997).

5. Marletta, M. A. Nitric oxide: biosynthesis and biological significance. *Trends Biochem. Sci.* **14,** 488–492 (1989).

6. Bredt, D. S. & Snyder, S. H. Nitric oxide: a physiologic messenger molecule. *Annu. Rev. Biochem.* **63,** 175–195 (1994).

7. Lowenstein, C. J., Dinerman, J. L. & Snyder, S. H. Nitric oxide: a physiologic messenger. *Ann. Intern. Med.* **120,** 227–237 (1994).

8. Shaul, P. W. Regulation of endothelial nitric oxide synthase: location, location, location. *Annu. Rev. Physiol.* **64,** 749–774 (2002).

9. Nathan, C. & Xie, Q. W. Nitric oxide synthases: roles, tolls, and controls. *Cell* **78,** 915–918 (1994).

10. Hemmens, B. & Mayer, B. Enzymology of nitric oxide synthases. *Methods Mol. Biol.* **100,** 1–32 (1998).

11. Crane, B. R. *et al.* Structure of nitric oxide synthase oxygenase dimer with pterin and substrate. *Science* **279,** 2121–2126 (1998).

12. Stuehr, D., Pou, S. & Rosen, G. M. Oxygen reduction by nitric-oxide synthases. *J. Biol. Chem.* **276,** 14533–14536 (2001).

13. Alderton, W. K., Cooper, C. E. & Knowles, R. G. Nitric oxide synthases: structure, function and inhibition. *Biochem. J.* **357,** 593–615 (2001).

14. Stuehr, D. J. Mammalian nitric oxide synthases. *Biochim. Biophys. Acta* **1411,** 217–230 (1999).

15. Cho, H. J. *et al.* Calmodulin is a subunit of nitric oxide synthase from macrophages. *J. Exp. Med.* **176,** 599–604 (1992).

16. Zhou, L. & Zhu, D.-Y. Neuronal nitric oxide synthase: structure, subcellular localization, regulation, and clinical implications. *Nitric Oxide* **20,** 223–230 (2009).

17. Förstermann, U. *et al.* Nitric oxide synthase isozymes. Characterization, purification, molecular cloning, and functions. *Hypertension* **23,** 1121–1131 (1994).

18. Izumi, Y., Clifford, D. B. & Zorumski, C. F. Inhibition of long-term potentiation by NMDA-mediated nitric oxide release. *Science* **257,** 1273–1276 (1992).

19. O'Dell, T. J., Hawkins, R. D., Kandel, E. R. & Arancio, O. Tests of the roles of two diffusible substances in long-term potentiation: evidence for nitric oxide as a possible early retrograde messenger. *Proc. Natl. Acad. Sci. USA* **88,** 11285–11289 (1991).

20. Hölscher, C. & Rose, S. P. An inhibitor of nitric oxide synthesis prevents memory formation in the chick. *Neurosci. Lett.* **145,** 165–167 (1992).

21. Steinert, J. R., Chernova, T. & Forsythe, I. D. Nitric oxide signaling in brain function, dysfunction, and dementia. *Neuroscientist* **16,** 435–452 (2010).

22. Lipton, S. A. *et al.* A redox-based mechanism for the neuroprotective and neurodestructive effects of nitric oxide and related nitroso-compounds. *Nature* **364,** 626–632 (1993).

23. Nathan, C. F. & Hibbs, J. B. Role of nitric oxide synthesis in macrophage antimicrobial activity. *Curr. Opin. Immunol.* **3,** 65–70 (1991).

24. Wink, D. A. *et al.* DNA deaminating ability and genotoxicity of nitric oxide and its progenitors. *Science* **254,** 1001–1003 (1991).

25. Xu, W., Liu, L. Z., Loizidou, M., Ahmed, M. & Charles, I. G. The role of nitric oxide in cancer. *Cell Res.* **12,** 311–320 (2002).

26. Salimian Rizi, B., Achreja, A. & Nagrath, D. Nitric oxide: the forgotten child of tumor metabolism. *Trends Cancer* **3,** 659–672 (2017).

27. Wink, D. A. *et al.* Nitric oxide and redox mechanisms in the immune response. *J. Leukoc. Biol.* **89,** 873–891 (2011).

28. Li, L. M., Kilbourn, R. G., Adams, J. & Fidler, I. J. Role of nitric oxide in lysis of tumor cells by cytokine-activated endothelial cells. *Cancer Res.* **51,** 2531–2535 (1991).

29. Green, S. J., Mellouk, S., Hoffman, S. L., Meltzer, M. S. & Nacy, C. A. Cellular mechanisms of nonspecific immunity to intracellular infection: cytokine-induced synthesis of toxic nitrogen oxides from L-arginine by macrophages and hepatocytes. *Immunol. Lett.* **25,** 15–19 (1990).

30. Fukumura, D., Kashiwagi, S. & Jain, R. K. The role of nitric oxide in tumour progression. *Nat. Rev. Cancer* **6,** 521–534 (2006).

31. Choudhari, S. K., Chaudhary, M., Bagde, S., Gadbail, A. R. & Joshi, V. Nitric oxide and cancer: a review. *World J Surg Oncol* **11,** 118 (2013).

32. Fehsel, K. *et al.* Islet cell DNA is a target of inflammatory attack by nitric oxide. *Diabetes* **42,** 496–500 (1993).

33. Kanwar, J. R., Kanwar, R. K., Burrow, H. & Baratchi, S. Recent advances on the roles of NO in cancer and chronic inflammatory disorders. *Curr. Med. Chem.* **16,** 2373–2394 (2009).

34. Brown, G. C. & Neher, J. J. Inflammatory neurodegeneration and mechanisms of microglial killing of neurons. *Mol. Neurobiol.* **41,** 242–247 (2010).

35. MacMicking, J. D. *et al.* Altered responses to bacterial infection and endotoxic shock in mice lacking inducible nitric oxide synthase. *Cell* **81,** 641–650 (1995).

36. Lange, M., Enkhbaatar, P., Nakano, Y. & Traber, D. L. Role of nitric oxide in shock: the large animal perspective. *Front. Biosci. (Landmark Ed)* **14,** 1979–1989 (2009).

37. Sowa, G. *et al.* Trafficking of endothelial nitric-oxide synthase in living cells. Quantitative evidence supporting the role of palmitoylation as a kinetic trapping mechanism limiting membrane diffusion. *J. Biol. Chem.* **274,** 22524–22531 (1999).

38. Sessa, W. C. *et al.* The Golgi association of endothelial nitric oxide synthase is necessary for the efficient synthesis of nitric oxide. *J. Biol. Chem.* **270,** 17641–17644 (1995).

39. Liu, J., Hughes, T. E. & Sessa, W. C. The first 35 amino acids and fatty acylation sites determine the molecular targeting of endothelial nitric oxide synthase into the Golgi region of cells: a green fluorescent protein study. *J. Cell Biol.* **137,** 1525–1535 (1997).

40. García-Cardeña, G., Oh, P., Liu, J., Schnitzer, J. E. & Sessa, W. C. Targeting of nitric oxide synthase to endothelial cell caveolae via palmitoylation: implications for nitric oxide signaling. *Proc. Natl. Acad. Sci. USA* **93,** 6448–6453 (1996).

41. Fulton, D. *et al.* Targeting of endothelial nitric-oxide synthase to the cytoplasmic face of the Golgi complex or plasma membrane regulates Akt- versus calcium-dependent mechanisms for nitric oxide release. *J. Biol. Chem.* **279,** 30349–30357 (2004).

42. Fulton, D. *et al.* Localization of endothelial nitric-oxide synthase phosphorylated on serine 1179 and nitric oxide in Golgi and plasma membrane defines the existence of two pools of active enzyme. *J. Biol. Chem.* **277,** 4277–4284 (2002).

43. García-Cardeña, G. *et al.* Dynamic activation of endothelial nitric oxide synthase by Hsp90. *Nature* **392,** 821–824 (1998).

44. Gratton, J. P. *et al.* Reconstitution of an endothelial nitric-oxide synthase (eNOS), hsp90, and caveolin-1 complex in vitro. Evidence that hsp90 facilitates calmodulin stimulated displacement of eNOS from caveolin-1. *J. Biol. Chem.* **275,** 22268–22272 (2000).

45. Ju, H., Zou, R., Venema, V. J. & Venema, R. C. Direct interaction of endothelial nitric-oxide synthase and caveolin-1 inhibits synthase activity. *J. Biol. Chem.* **272,** 18522–18525 (1997).

46. Drab, M. *et al.* Loss of caveolae, vascular dysfunction, and pulmonary defects in caveolin-1 gene-disrupted mice. *Science* **293,** 2449–2452 (2001).

47. Fleming, I. & Busse, R. Molecular mechanisms involved in the regulation of the endothelial nitric oxide synthase. *Am. J. Physiol. Regul. Integr. Comp. Physiol.* **284,** R1–12 (2003).

48. Fulton, D. *et al.* Regulation of endothelium-derived nitric oxide production by the protein kinase Akt. *Nature* **399,** 597–601 (1999).

49. Fulton, D., Gratton, J. P. & Sessa, W. C. Post-translational control of endothelial nitric oxide synthase: why isn't calcium/calmodulin enough? *J. Pharmacol. Exp. Ther.* **299,** 818–824 (2001).

50. McCabe, T. J., Fulton, D., Roman, L. J. & Sessa, W. C. Enhanced electron flux and reduced calmodulin dissociation may explain "calcium-independent" eNOS activation by phosphorylation. *J. Biol. Chem.* **275,** 6123–6128 (2000).

51. Schleicher, M. *et al.* The Akt1-eNOS axis illustrates the specificity of kinase-substrate relationships in vivo. *Sci. Signal.* **2,** ra41 (2009).

52. Lin, M. I. *et al.* Phosphorylation of threonine 497 in endothelial nitric-oxide synthase coordinates the coupling of L-arginine metabolism to efficient nitric oxide production. *J. Biol. Chem.* **278,** 44719–44726 (2003).

53. Fleming, I. Molecular mechanisms underlying the activation of eNOS. *Pflugers Arch.* **459,** 793–806 (2010).

54. Förstermann, U., Mülsch, A., Böhme, E. & Busse, R. Stimulation of soluble guanylate cyclase by an acetylcholine-induced endothelium-derived factor from rabbit and canine arteries. *Circ. Res.* **58,** 531–538 (1986).

55. Shesely, E. G. *et al.* Elevated blood pressures in mice lacking endothelial nitric oxide synthase. *Proc. Natl. Acad. Sci. USA* **93,** 13176–13181 (1996).

56. Radomski, M. W., Palmer, R. M. & Moncada, S. The anti-aggregating properties of vascular endothelium: interactions between prostacyclin and nitric oxide. *Br. J. Pharmacol.* **92,** 639–646 (1987).

57. Alheid, U., Frölich, J. C. & Förstermann, U. Endothelium-derived relaxing factor from cultured human endothelial cells inhibits aggregation of human platelets. *Thromb. Res.* **47,** 561–571 (1987).

58. Rudic, R. D. *et al.* Direct evidence for the importance of endothelium-derived nitric oxide in vascular remodeling. *J. Clin. Invest.* **101,** 731–736 (1998).

59. Förstermann, U. Oxidative stress in vascular disease: causes, defense mechanisms and potential therapies. *Nat. Clin. Pract. Cardiovasc. Med.* **5,** 338–349 (2008).

60. Han, R. N. N. & Stewart, D. J. Defective lung vascular development in endothelial nitric oxide synthase-deficient mice. *Trends Cardiovasc. Med.* **16,** 29–34 (2006).

61. Murohara, T. *et al.* Nitric oxide synthase modulates angiogenesis in response to tissue ischemia. *J. Clin. Invest.* **101,** 2567–2578 (1998).

62. Aicher, A. *et al.* Essential role of endothelial nitric oxide synthase for mobilization of stem and progenitor cells. *Nat. Med.* **9,** 1370–1376 (2003).

63. Ying, L. & Hofseth, L. J. An emerging role for endothelial nitric oxide synthase in chronic inflammation and cancer. *Cancer Res.* **67,** 1407–1410 (2007).

64. deRojas-Walker, T., Tamir, S., Ji, H., Wishnok, J. S. & Tannenbaum, S. R. Nitric oxide induces oxidative damage in addition to deamination in macrophage DNA. *Chem. Res. Toxicol.* **8,** 473–477 (1995).

65. Gal, A. & Wogan, G. N. Mutagenesis associated with nitric oxide production in transgenic SJL mice. *Proc. Natl. Acad. Sci. USA* **93,** 15102–15107 (1996).

66. Sun, Y. Free radicals, antioxidant enzymes, and carcinogenesis. *Free Radic. Biol. Med.* **8,** 583–599 (1990).

67. Choi, B.-M., Pae, H.-O., Jang, S. I., Kim, Y.-M. & Chung, H.-T. Nitric oxide as a pro-apoptotic as well as anti-apoptotic modulator. *J. Biochem. Mol. Biol.* **35,** 116–126 (2002).

68. Ziche, M. & Morbidelli, L. Nitric oxide and angiogenesis. *J. Neurooncol.* **50,** 139–148 (2000).

69. Lala, P. K. & Orucevic, A. Role of nitric oxide in tumor progression: lessons from experimental tumors. *Cancer Metastasis Rev.* **17,** 91–106 (1998).

70. Loibl, S. *et al.* Expression of endothelial and inducible nitric oxide synthase in benign and malignant lesions of the breast and measurement of nitric oxide using electron paramagnetic resonance spectroscopy. *Cancer* **95,** 1191–1198 (2002).

71. Lampson, B. L. *et al.* Targeting eNOS in pancreatic cancer. *Cancer Res.* **72,** 4472–4482 (2012).

72. Loibl, S. *et al.* Immunohistochemical evaluation of endothelial nitric oxide synthase expression in primary breast cancer. *Breast* **14,** 230–235 (2005).

73. Thomsen, L. L. *et al.* Nitric oxide synthase activity in human breast cancer. *Br. J. Cancer* **72,** 41–44 (1995).

74. Jadeski, L. C., Hum, K. O., Chakraborty, C. & Lala, P. K. Nitric oxide promotes murine mammary tumour growth and metastasis by stimulating tumour cell migration, invasiveness and angiogenesis. *Int. J. Cancer* **86,** 30–39 (2000).

75. Nakamura, Y. *et al.* Nitric oxide in breast cancer: induction of vascular endothelial growth factor-C and correlation with metastasis and poor prognosis. *Clin. Cancer Res.* **12,** 1201–1207 (2006).

76. Tschugguel, W. *et al.* Expression of inducible nitric oxide synthase in human breast cancer depends on tumor grade. *Breast Cancer Res. Treat.* **56,** 145–151 (1999).

77. Tschugguel, W. *et al.* Presence of endothelial calcium-dependent nitric oxide synthase in breast apocrine metaplasia. *Br. J. Cancer* **74,** 1423–1426 (1996).

78. Zeillinger, R. *et al.* Simultaneous expression of nitric oxide synthase and estrogen receptor in human breast cancer cell lines. *Breast Cancer Res. Treat.* **40,** 205–207 (1996).

79. Pance, A. Nitric oxide and hormones in breast cancer: allies or enemies? *Future Oncol* **2,** 275–288 (2006).

80. Bentrari, F., Arnould, L., Jackson, A. P., Jeannin, J.-F. & Pance, A. Progesterone enhances cytokine-stimulated nitric oxide synthase II expression and cell death in human breast cancer cells. *Lab. Invest.* **85,** 624–632 (2005).

81. Ye, X., Rubakhin, S. S. & Sweedler, J. V. Detection of nitric oxide in single cells. *Analyst* **133,** 423–433 (2008).

82. Thomas, D. D., Liu, X., Kantrow, S. P. & Lancaster, J. R. The biological lifetime of nitric oxide: Implications for the perivascular dynamics of NO and O2. *Proc. Natl. Acad. Sci. USA* **98,** 355–360 (2001).

83. Eroglu, E. *et al.* Genetic biosensors for imaging nitric oxide in single cells. *Free Radic. Biol. Med.* **128,** 50–58 (2018).

84. Yoshimura, T. *et al.* In vivo EPR detection and imaging of endogenous nitric oxide in lipopolysaccharide-treated mice. *Nat. Biotechnol.* **14,** 992–994 (1996).

85. Leone, A. M., Furst, V. W., Foxwell, N. A., Cellek, S. & Moncada, S. Visualisation of nitric oxide generated by activated murine macrophages. *Biochem. Biophys. Res. Commun.* **221,** 37–41 (1996).

86. Kojima, H. *et al.* Detection and imaging of nitric oxide with novel fluorescent indicators: diaminofluoresceins. *Anal. Chem.* **70,** 2446–2453 (1998).

87. Nakatsubo, N. *et al.* Direct evidence of nitric oxide production from bovine aortic endothelial cells using new fluorescence indicators: diaminofluoresceins. *FEBS Lett.* **427,** 263–266 (1998).

88. Lacza, Z. *et al.* Lack of mitochondrial nitric oxide production in the mouse brain. *J. Neurochem.* **90,** 942–951 (2004).

89. Leikert, J. F., Räthel, T. R., Müller, C., Vollmar, A. M. & Dirsch, V. M. Reliable in vitro measurement of nitric oxide released from endothelial cells using low concentrations of the fluorescent probe 4,5-diaminofluorescein. *FEBS Lett.* **506,** 131–134 (2001).

90. Mainz, E. R. *et al.* Monitoring intracellular nitric oxide production using microchip electrophoresis and laser-induced fluorescence detection. *Anal. Methods* **4,** 414 (2012).

91. Eroglu, E. *et al.* Development of novel FP-based probes for live-cell imaging of nitric oxide dynamics. *Nat. Commun.* **7,** 10623 (2016).

92. Modi, S. *et al.* A DNA nanomachine that maps spatial and temporal pH changes inside living cells. *Nat. Nanotechnol.* **4,** 325–330 (2009).

93. Modi, S., Nizak, C., Surana, S., Halder, S. & Krishnan, Y. Two DNA nanomachines map pH changes along intersecting endocytic pathways inside the same cell. *Nat. Nanotechnol.* **8,** 459–467 (2013).

94. Surana, S., Bhat, J. M., Koushika, S. P. & Krishnan, Y. An autonomous DNA nanomachine maps spatiotemporal pH changes in a multicellular living organism. *Nat. Commun.* **2,** 340 (2011).

95. Chakraborty, K., Leung, K. & Krishnan, Y. High lumenal chloride in the lysosome is critical for lysosome function. *Elife* **6,** e28862 (2017).

96. Narayanaswamy, N. *et al.* A pH-correctable, DNA-based fluorescent reporter for organellar calcium. *Nat. Methods* **16,** 95–102 (2019).

97. Dan, K., Veetil, A. T., Chakraborty, K. & Krishnan, Y. DNA nanodevices map enzymatic activity in organelles. *Nat. Nanotechnol.* **14,** 252–259 (2019).

98. Thekkan, S. *et al.* A DNA-based fluorescent reporter maps HOCl production in the maturing phagosome. *Nat. Chem. Biol.* **15,** 1165–1172 (2019).

99. Sharma, S., Zajac, M. & Krishnan, Y. A DNA Aptamer for Cyclic Adenosine Monophosphate that Shows Adaptive Recognition. *Chembiochem* **21,** 157–162 (2020).

100. Saminathan, A. *et al.* A DNA-based voltmeter for organelles: Supplementary information. *BioRxiv* (2019). doi:10.1101/523019

101. Leung, K., Chakraborty, K., Saminathan, A. & Krishnan, Y. A DNA nanomachine chemically resolves lysosomes in live cells. *Nat. Nanotechnol.* **14,** 176–183 (2019).

102. Jani, M. S., Veetil, A. T. & Krishnan, Y. Precision immunomodulation with synthetic nucleic acid technologies. *Nat. Rev. Mater.* (2019). doi:10.1038/s41578-019-0105-4

103. Saha, S., Prakash, V., Halder, S., Chakraborty, K. & Krishnan, Y. A pH-independent DNA nanodevice for quantifying chloride transport in organelles of living cells. *Nat. Nanotechnol.* **10,** 645–651 (2015).

104. Jani, M. S., Zou, J., Veetil, A. T. & Krishnan, Y. A DNA-based fluorescent probe maps NOS3 activity with subcellular spatial resolution. *Nat. Chem. Biol.* **16,** 660–666 (2020).

105. Kojima, H. *et al.* Bioimaging of nitric oxide with fluorescent indicators based on the rhodamine chromophore. *Anal. Chem.* **73,** 1967–1973 (2001).

106. Nagano, T. & Yoshimura, T. Bioimaging of nitric oxide. *Chem. Rev.* **102,** 1235–1270 (2002).

107. Panchuk-Voloshina, N. *et al.* Alexa Dyes, a Series of New Fluorescent Dyes that Yield Exceptionally Bright, Photostable Conjugates. *Journal of Histochemistry & Cytochemistry* **47,** 1179–1188 (1999).

108. You, M. *et al.* DNA probes for monitoring dynamic and transient molecular encounters on live cell membranes. *Nat. Nanotechnol.* **12,** 453–459 (2017).

109. Pfeiffer, I. & Höök, F. Bivalent cholesterol-based coupling of oligonucletides to lipid membrane assemblies. *J. Am. Chem. Soc.* **126,** 10224–10225 (2004).

110. Ferreira, C. S. M., Cheung, M. C., Missailidis, S., Bisland, S. & Gariépy, J. Phototoxic aptamers selectively enter and kill epithelial cancer cells. *Nucleic Acids Res.* **37,** 866–876 (2009).

111. Heinlein, T., Knemeyer, J.-P., Piestert, O. & Sauer, M. Photoinduced Electron Transfer between Fluorescent Dyes and Guanosine Residues in DNA-Hairpins. *J. Phys. Chem. B* **107,** 7957–7964 (2003).

112. Yao, L., Smith, B. T. & Aubé, J. Base-promoted reactions of bridged ketones and 1,3- and 1,4-haloalkyl azides: competitive alkylation vs azidation reactions of ketone enolates. *J. Org. Chem.* **69,** 1720–1722 (2004).

113. Schindelin, J. *et al.* Fiji: an open-source platform for biological-image analysis. *Nat. Methods* **9,** 676–682 (2012).

114. Brandes, R. P. & Janiszewski, M. Direct detection of reactive oxygen species ex vivo. *Kidney Int.* **67,** 1662–1664 (2005).

115. Duarte, A. J. & da Silva, J. C. G. E. Reduced fluoresceinamine as a fluorescent sensor for nitric oxide. *Sensors (Basel)* **10,** 1661–1669 (2010).

116. Goldstein, S., Russo, A. & Samuni, A. Reactions of PTIO and carboxy-PTIO with *NO, *NO2, and O2-*. *J. Biol. Chem.* **278,** 50949–50955 (2003).

117. Iwasaki, T. *et al.* NG-nitro-L-arginine methyl ester inhibits bone metastasis after modified intracardiac injection of human breast cancer cells in a nude mouse model. *Jpn. J. Cancer Res.* **88,** 861–866 (1997).

118. Garvey, E. P. *et al.* 1400W is a slow, tight binding, and highly selective inhibitor of inducible nitric-oxide synthase in vitro and in vivo. *J. Biol. Chem.* **272,** 4959–4963 (1997).

119. Zhang, Q. *et al.* Functional relevance of Golgi- and plasma membrane-localized endothelial NO synthase in reconstituted endothelial cells. *Arterioscler. Thromb. Vasc. Biol.* **26,** 1015–1021 (2006).

120. Veetil, A. T., Jani, M. S. & Krishnan, Y. Chemical control over membrane-initiated steroid signaling with a DNA nanocapsule. *Proc. Natl. Acad. Sci. USA* **115,** 9432–9437 (2018).

121. Eroglu, E., Michel, T., Graier, W. F. & Malli, R. Yes (again) to local NO. *Nat. Chem. Biol.* **16,** 606–607 (2020).

122. Bagheri, Y., Chedid, S., Shafiei, F., Zhao, B. & You, M. A quantitative assessment of the dynamic modification of lipid-DNA probes on live cell membranes. *Chem. Sci.* **10,** 11030–11040 (2019).

123. Weber, R. J., Liang, S. I., Selden, N. S., Desai, T. A. & Gartner, Z. J. Efficient targeting of fatty-acid modified oligonucleotides to live cell membranes through stepwise assembly. *Biomacromolecules* **15,** 4621–4626 (2014).

124. Engelmann, K. *et al.* Transmembrane and secreted MUC1 probes show trafficking-dependent changes in O-glycan core profiles. *Glycobiology* **15,** 1111–1124 (2005).

125. Litvinov, S. V. & Hilkens, J. The epithelial sialomucin, episialin, is sialylated during recycling. *J. Biol. Chem.* **268,** 21364–21371 (1993).

126. Eroglu, E., Saravi, S. S. S., Sorrentino, A., Steinhorn, B. & Michel, T. Discordance between eNOS phosphorylation and activation revealed by multispectral imaging and chemogenetic methods. *Proc. Natl. Acad. Sci. USA* **116,** 20210–20217 (2019).

127. Modi, S., Halder, S., Nizak, C. & Krishnan, Y. Recombinant antibody mediated delivery of organelle-specific DNA pH sensors along endocytic pathways. *Nanoscale* **6,** 1144–1152 (2014).

128. Hess, D. T., Matsumoto, A., Kim, S.-O., Marshall, H. E. & Stamler, J. S. Protein S-nitrosylation: purview and parameters. *Nat. Rev. Mol. Cell Biol.* **6,** 150–166 (2005).

129. Sangwung, P. *et al.* Proteomic identification of S-nitrosylated Golgi proteins: new insights into endothelial cell regulation by eNOS-derived NO. *PLoS One* **7,** e31564 (2012).

130. Wang, Z. Protein S-nitrosylation and cancer. *Cancer Lett.* **320,** 123–129 (2012).

131. Sowa, G., Pypaert, M. & Sessa, W. C. Distinction between signaling mechanisms in lipid rafts vs. caveolae. *Proc. Natl. Acad. Sci. USA* **98,** 14072–14077 (2001).

132. Lim, K.-H., Ancrile, B. B., Kashatus, D. F. & Counter, C. M. Tumour maintenance is mediated by eNOS. *Nature* **452,** 646–649 (2008).

133. Jin, Z.-G. Where is endothelial nitric oxide synthase more critical: plasma membrane or Golgi? *Arterioscler. Thromb. Vasc. Biol.* **26,** 959–961 (2006).

134. Namin, S. M., Nofallah, S., Joshi, M. S., Kavallieratos, K. & Tsoukias, N. M. Kinetic analysis of DAF-FM activation by NO: toward calibration of a NO-sensitive fluorescent dye. *Nitric Oxide* **28,** 39–46 (2013).

135. Awad, H. H. & Stanbury, D. M. Autoxidation of NO in aqueous solution. *Int. J. Chem. Kinet.* **25,** 375–381 (1993).

136. Ramamurthi, A. & Lewis, R. S. Measurement and modeling of nitric oxide release rates for nitric oxide donors. *Chem. Res. Toxicol.* **10,** 408–413 (1997).

137. Lewis, R. S. & Deen, W. M. Kinetics of the reaction of nitric oxide with oxygen in aqueous solutions. *Chem. Res. Toxicol.* **7,** 568–574 (1994).

138. Roy, B., du Moulinet d'Hardemare, A. & Fontecave, M. New thionitrites: synthesis, stability, and nitric oxide generation. *J. Org. Chem.* **59,** 7019–7026 (1994).

139. Lytton, J., Westlin, M. & Hanley, M. R. Thapsigargin inhibits the sarcoplasmic or endoplasmic reticulum Ca-ATPase family of calcium pumps. *J. Biol. Chem.* **266,** 17067–17071 (1991).

140. Jiang, S. *et al.* Real-time electrical detection of nitric oxide in biological systems with sub-nanomolar sensitivity. *Nat. Commun.* **4,** 2225 (2013).

141. Feng, J., Chen, L. & Zuo, J. Protein S-Nitrosylation in plants: Current progresses and challenges. *J. Integr. Plant Biol.* **61,** 1206–1223 (2019).

142. Crane, B. R., Sudhamsu, J. & Patel, B. A. Bacterial nitric oxide synthases. *Annu. Rev. Biochem.* **79,** 445–470 (2010).

143. Murad, F. Cyclic guanosine monophosphate as a mediator of vasodilation. *J. Clin. Invest.* **78,** 1–5 (1986).

144. Stamler, J. S., Singel, D. J. & Loscalzo, J. Biochemistry of nitric oxide and its redox-activated forms. *Science* **258,** 1898–1902 (1992).

145. Stamler, J. S. *et al.* S-nitrosylation of proteins with nitric oxide: synthesis and characterization of biologically active compounds. *Proc. Natl. Acad. Sci. USA* **89,** 444–448 (1992).

146. Lee, T.-Y. *et al.* dbSNO: a database of cysteine S-nitrosylation. *Bioinformatics* **28,** 2293–2295 (2012).

147. Jaffrey, S. R., Erdjument-Bromage, H., Ferris, C. D., Tempst, P. & Snyder, S. H. Protein S-nitrosylation: a physiological signal for neuronal nitric oxide. *Nat. Cell Biol.* **3,** 193–197 (2001).

148. Liu, L. *et al.* Essential roles of S-nitrosothiols in vascular homeostasis and endotoxic shock. *Cell* **116,** 617–628 (2004).

149. de Jesús-Berríos, M. *et al.* Enzymes that counteract nitrosative stress promote fungal virulence. *Curr. Biol.* **13,** 1963–1968 (2003).

150. Hess, D. T., Matsumoto, A., Nudelman, R. & Stamler, J. S. S-nitrosylation: spectrum and specificity. *Nat. Cell Biol.* **3,** E46–9 (2001).

151. Aranda, E., López-Pedrera, C., De La Haba-Rodriguez, J. R. & Rodriguez-Ariza, A. Nitric oxide and cancer: the emerging role of S-nitrosylation. *Curr. Mol. Med.* **12,** 50–67 (2012).

152. Mannick, J. B. *et al.* Fas-induced caspase denitrosylation. *Science* **284,** 651–654 (1999).

153. Rahman, M. A. *et al.* S-nitrosylation at cysteine 498 of c-Src tyrosine kinase regulates nitric oxide-mediated cell invasion. *J. Biol. Chem.* **285,** 3806–3814 (2010).

154. Hao, L., Wei, X., Guo, P., Zhang, G. & Qi, S. Neuroprotective Effects of Inhibiting Fyn S-Nitrosylation on Cerebral Ischemia/Reperfusion-Induced Damage to CA1 Hippocampal Neurons. *Int. J. Mol. Sci.* **17,** (2016).

155. Heo, J. & Campbell, S. L. Mechanism of p21Ras S-nitrosylation and kinetics of nitric oxide-mediated guanine nucleotide exchange. *Biochemistry* **43,** 2314–2322 (2004).

156. Azad, N. *et al.* S-nitrosylation of Bcl-2 inhibits its ubiquitin-proteasomal degradation. A novel antiapoptotic mechanism that suppresses apoptosis. *J. Biol. Chem.* **281,** 34124–34134 (2006).

157. Calmels, S., Hainaut, P. & Ohshima, H. Nitric oxide induces conformational and functional modifications of wild-type p53 tumor suppressor protein. *Cancer Res.* **57,** 3365–3369 (1997).

158. Guan, W. *et al.* S-Nitrosylation of mitogen activated protein kinase phosphatase-1 suppresses radiation-induced apoptosis. *Cancer Lett.* **314,** 137–146 (2012).

159. Leon-Bollotte, L. *et al.* S-nitrosylation of the death receptor fas promotes fas ligand-mediated apoptosis in cancer cells. *Gastroenterology* **140,** 2009–18, 2018.e1 (2011).

160. Lima, B. *et al.* Endogenous S-nitrosothiols protect against myocardial injury. *Proc. Natl. Acad. Sci. USA* **106,** 6297–6302 (2009).

161. Kang-Decker, N. *et al.* Nitric oxide promotes endothelial cell survival signaling through S-nitrosylation and activation of dynamin-2. *J. Cell Sci.* **120,** 492–501 (2007).

162. Pi, X., Wu, Y., Ferguson, J. E., Portbury, A. L. & Patterson, C. SDF-1alpha stimulates JNK3 activity via eNOS-dependent nitrosylation of MKP7 to enhance endothelial migration. *Proc. Natl. Acad. Sci. USA* **106,** 5675–5680 (2009).

163. Yu, C.-X., Li, S. & Whorton, A. R. Redox regulation of PTEN by S-nitrosothiols. *Mol. Pharmacol.* **68,** 847–854 (2005).

164. Liu, L., Xu-Welliver, M., Kanugula, S. & Pegg, A. Inactivation and Degradation of O6-Alkylguanine-DNA Alkyltransferase after Reaction with Nitric Oxide1.

165. Iwakiri, Y. *et al.* Nitric oxide synthase generates nitric oxide locally to regulate compartmentalized protein S-nitrosylation and protein trafficking. *Proc. Natl. Acad. Sci. USA* **103,** 19777–19782 (2006).

166. Barouch, L. A. *et al.* Nitric oxide regulates the heart by spatial confinement of nitric oxide synthase isoforms. *Nature* **416,** 337–339 (2002).

167. Boehning, D. & Snyder, S. H. Novel neural modulators. *Annu. Rev. Neurosci.* **26,** 105–131 (2003).

168. Stamler, J. S., Lamas, S. & Fang, F. C. Nitrosylation. the prototypic redox-based signaling mechanism. *Cell* **106,** 675–683 (2001).

169. Bartberger, M. D. *et al.* S-N dissociation energies of S-nitrosothiols: on the origins of nitrosothiol decomposition rates. *J. Am. Chem. Soc.* **123,** 8868–8869 (2001).

170. Stamler, J. S. & Toone, E. J. The decomposition of thionitrites. *Curr. Opin. Chem. Biol.* **6,** 779–785 (2002).

171. Romeo, A. A., Capobianco, J. A. & English, A. M. Superoxide dismutase targets NO from GSNO to Cysbeta93 of oxyhemoglobin in concentrated but not dilute solutions of the protein. *J. Am. Chem. Soc.* **125,** 14370–14378 (2003).

172. Benhar, M., Forrester, M. T. & Stamler, J. S. Protein denitrosylation: enzymatic mechanisms and cellular functions. *Nat. Rev. Mol. Cell Biol.* **10,** 721–732 (2009).

173. Vahora, H., Khan, M. A., Alalami, U. & Hussain, A. The potential role of nitric oxide in halting cancer progression through chemoprevention. *J. Cancer Prev.* **21,** 1–12 (2016).

174. Farber-Katz, S. E. *et al.* DNA damage triggers Golgi dispersal via DNA-PK and GOLPH3. *Cell* **156,** 413–427 (2014).

175. Debacq-Chainiaux, F., Erusalimsky, J. D., Campisi, J. & Toussaint, O. Protocols to detect senescence-associated beta-galactosidase (SA-betagal) activity, a biomarker of senescent cells in culture and in vivo. *Nat. Protoc.* **4,** 1798–1806 (2009).

176. Lee, J. E. *et al.* Dependence of Golgi apparatus integrity on nitric oxide in vascular cells: implications in pulmonary arterial hypertension. *Am. J. Physiol. Heart Circ. Physiol.* **300,** H1141–58 (2011).

177. Damiens, E., Baratte, B., Marie, D., Eisenbrand, G. & Meijer, L. Anti-mitotic properties of indirubin-3'-monoxime, a CDK/GSK-3 inhibitor: induction of endoreplication following prophase arrest. *Oncogene* **20,** 3786–3797 (2001).

178. Blake, R. A. *et al.* SU6656, a selective src family kinase inhibitor, used to probe growth factor signaling. *Mol. Cell. Biol.* **20,** 9018–9027 (2000).

179. Skupien, A. *et al.* CD44 regulates dendrite morphogenesis through Src tyrosine kinase-dependent positioning of the Golgi. *J. Cell Sci.* **127,** 5038–5051 (2014).